reaction temperature, on physical properties of the synthesized nanorods as well as the mechanism were investigated. An interesting correlation between aspect ratio of the ZnO products and physical properties of the solvent was observed and presented in this work.

## 2. Experiment

### 2.1. Preparation of ZnO

Zinc acetate ($Zn(CH_3CO_2)_2$) in a predetermined amount in the range of 10–25 g was suspended in 100 ml of alcohol in a glass vessel, which was then placed in a 300 ml autoclave. Alcohols used in this work were 1-butanol, 1-hexanol, 1-octanol and 1-decanol, respectively. The gap between autoclave wall and the glass vessel was filled with 30 ml of the same alcohol. The autoclave was completely sealed and purged with nitrogen. The mixture was heated to desired temperature, in the range of 250–300 °C, at a constant heating rate of 2.5 °C/min, and held at that temperature for 2 h. Subsequently, after the autoclave was cooled, the product obtained in the vessel was collected by centrifugation, washed with methanol and dried in air at room temperature.

### 2.2. Characterization

The prepared samples were examined by X-ray diffraction (XRD) analysis using a SIEMENS XRD D500 diffractometer with Cu Kα radiation. The morphology and crystallite size of the nanoparticles were observed on a JEOL JSM6400 Scanning Electron Microscope (SEM) and a JEOL JEM1220 Transmission Electron Microscope (TEM). Infrared spectra of the products were also obtained using Nicolet FT-IR spectrophotometer model Impact 400. Each sample was mixed with KBr in the ratio of 1:100 and then pressed into a thin pellet. Infrared spectra were recorded at wave number in the range of 400 and 4000 $cm^{-1}$.

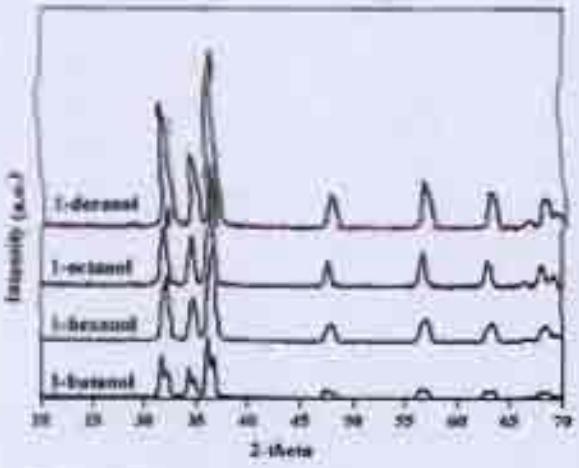


Fig. 1. The X-ray diffraction patterns of ZnO powder prepared by solvothermal reaction at 250 °C for 2 h in various alcohols.

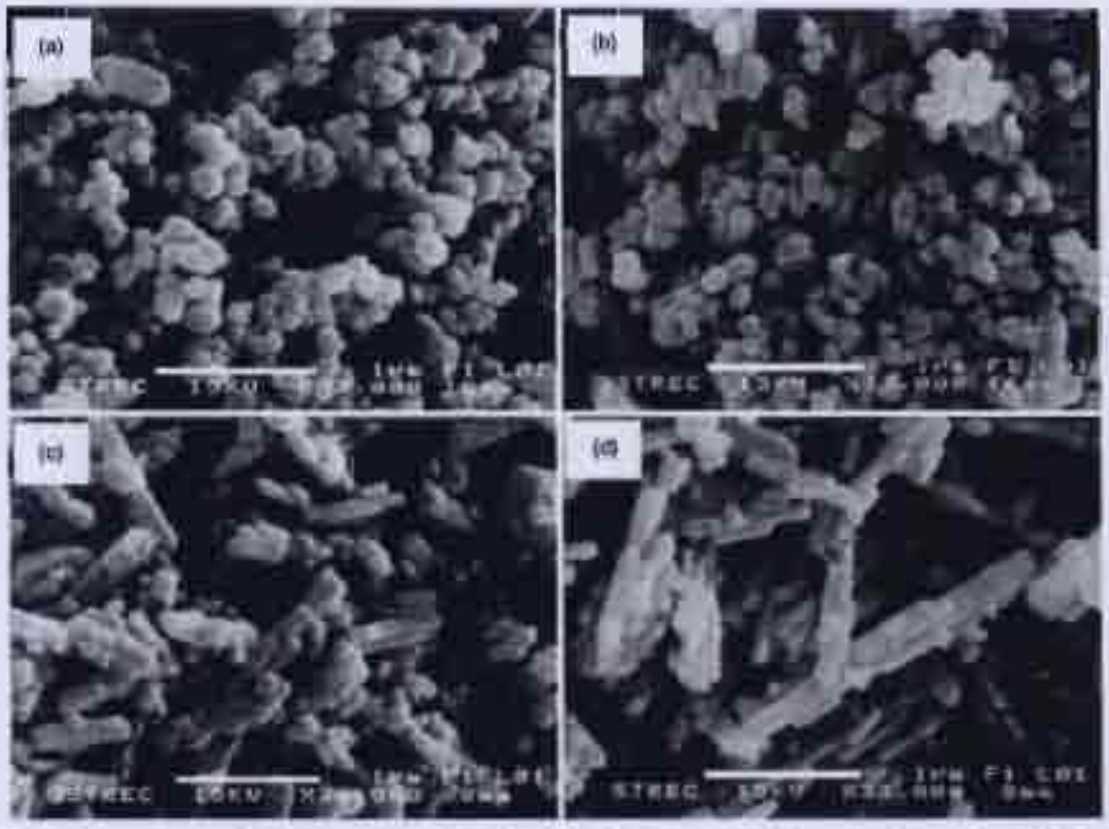


Fig. 2. SEM images of as-synthesized ZnO synthesized at 250 °C for 2 h in: (a) 1-butanol, (b) 1-hexanol, (c) 1-octanol and (d) 1-decanol.

Please cite this article in press as: P. Tonto et al., Preparation of ZnO nanorod by solvothermal reaction of zinc acetate in various alcohols, Ceram. Int. (2006), doi:10.1016/j.ceramint.2006.05.003

## 3. Results and discussion

### 3.1. Effect of various reaction conditions

XRD patterns of powders synthesized by the solvothermal reaction in various alcohols at 250 °C are shown in Fig. 1. All peaks of the obtained product were corresponding to the hexagonal wurtzite structure of ZnO with lattice parameters $a$ and $c$ of 3.24 and 5.19 Å, respectively. No peak from either ZnO in other phases or impurities was observed. This result confirmed that ZnO was successfully synthesized by the solvothermal reaction in all alcohols investigated. Nevertheless, it should be noted that the XRD pattern of the product synthesized in 1-butanol showed slight split for all XRD peaks, which suggested non-homogeneity in the crystal structure of the ZnO product.

Fig. 2a–d show SEM images of the products synthesized in 1-butanol, 1-hexanol, 1-octanol and 1-decanol, respectively. It was clearly illustrated that morphology of particles synthesized in these alcohols were significantly different. Nearly spherical particles were obtained when 1-butanol was used as the reaction medium, while smooth solid hexagonal rods were observed in the product prepared in 1-decanol. Therefore, it could be taken that the product from the solvothermal synthesis in alcohol was ZnO nanorods and the length of the rods increased when alcohol with longer molecule was employed.

Morphology of the primary ZnO particle was examined from TEM images, as shown in Fig. 3. The results confirmed with SEM observation that nanorods synthesized were straight and non-porous. The selected area electron diffraction (SAED) patterns shown as the inset in Fig. 3 suggested that each primary particle was a rod-shaped single crystal of ZnO. The observed morphology was consistent with the hexagonal nanorods grown in 0 0 1 direction. It was also found that all synthesized ZnO nanorods were quite uniform in size. The distributions of diameter of the rods measured from TEM micrographs are shown in Fig. 4. According to Fig. 4, it was shown that the synthesized ZnO nanorods had narrow size distribution, regardless of the type of alcohol employed. The average diameter and length as well as the calculated aspect ratio of the particles are summarized in Table 1.

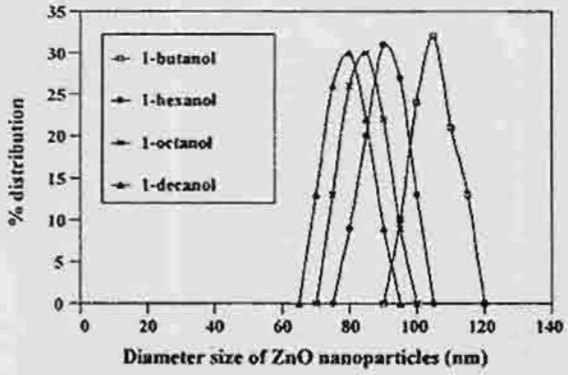


Fig. 4. The size distributions for diameter of ZnO nanorods synthesized in: (a) 1-butanol, (b) 1-hexanol, (c) 1-octanol and (d) 1-decanol.

According to Table 1, ZnO synthesized in alcohol having long carbon chain tended to be nanorods that were longer and had

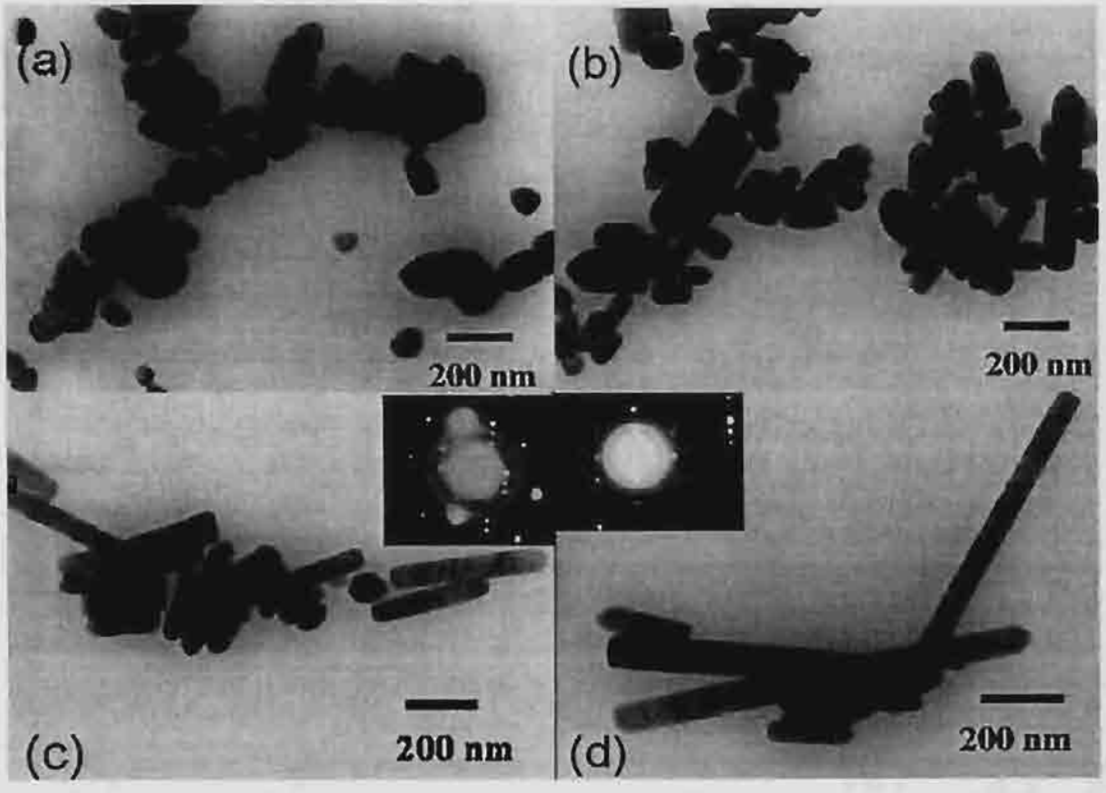


Fig. 3. TEM images of as-synthesized ZnO synthesized in: (a) 1-butanol, (b) 1-hexanol, (c) 1-octanol and (d) 1-decanol.

Please cite this article in press as: P. Tonto et al., Preparation of ZnO nanorod by solvothermal reaction of zinc acetate in various alcohols, Ceram. Int. (2006), doi:10.1016/j.ceramint.2006.08.003

Table 1
The crystallite size and aspect ratio of ZnO nanorods

| Solvent | Synthesis emperature (°C) | Amount of zinc acetate used (g) | Average diameter of product (nm) | Average length (nm) | Aspect ratio |
|---|---|---|---|---|---|
| 1-Butanol | 250 | 15 | 107 | 184 | 1.7 |
| 1-Hexanol | 250 | 15 | 91 | 264 | 2.9 |
| 1-Octanol | 200 | 15 | 67 | 284 | 4.2 |
| 1-Octanol | 230 | 15 | 75 | 308 | 4.1 |
| 1-Octanol | 250 | 10 | 79 | 316 | 4.0 |
| 1-Octanol | 250 | 15 | 84 | 343 | 4.1 |
| 1-Octanol | 250 | 20 | 97 | 385 | 4.0 |
| 1-Octanol | 300 | 15 | 110 | 472 | 4.3 |
| 1-Decanol | 200 | 15 | 69 | 392 | 5.7 |
| 1-Decanol | 230 | 15 | 74 | 419 | 5.7 |
| 1-Decanol | 250 | 10 | 76 | 423 | 5.6 |
| 1-Decanol | 250 | 15 | 81 | 455 | 5.6 |
| 1-Decanol | 250 | 20 | 91 | 506 | 5.6 |

diameter smaller than those synthesized in short-chain alcohol. The aspect ratio of the obtained nanorods increased corresponding to an increase in length of the carbon chain of the reaction medium. When 1-decanol was used instead of 1-butanol, the length of nanorods increased from 184 to 455 nm, while the average diameter decreased from 107 to 81 nm. Consequently, the aspect ratio increased approximately three-fold.

Table 1 also summarizes dimension of ZnO particles synthesized under various reaction conditions. It was found that both average diameter and length of the ZnO nanorods increased with an increase in either initial concentration of the precursor (i.e. zinc acetate) or reaction temperature. This observation suggested the increase in crystal growth with number of nuclei sites as well as the energy of the system. However, it should be noted that the aspect ratio of ZnO particles was not affected by either the temperature or amount of precursor. In the other words, the change in the reaction conditions did not alter the growth of ZnO nanoparticles into preferential orientation. Type of alcohol employed as the reaction medium was the only major factor affecting the aspect ratio of the synthesized particles.

The aspect ratio of ZnO nanorod was determined from relative growth rates from various faces of the crystal. The rate of crystal

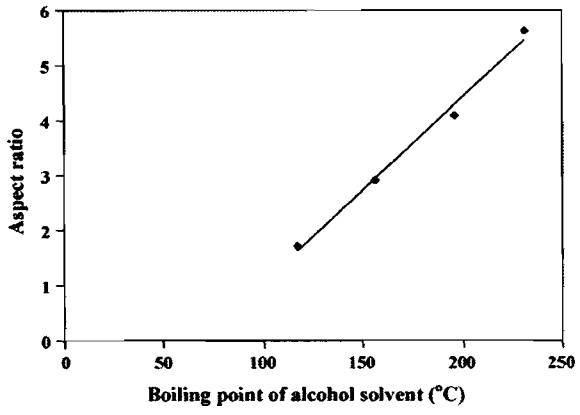


Fig. 5. The correlation between boiling points of the employed solvent and aspect ratio of ZnO products.

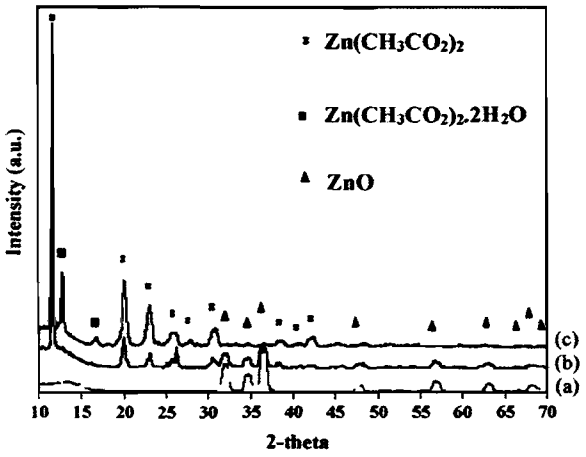


Fig. 6. The X-ray diffraction patterns of: (a) the reaction precursor, i.e. zinc acetate, (b) ZnO synthesized in 1-octanol at 150 °C and (c) ZnO synthesized in 1-octanol at 200 °C.

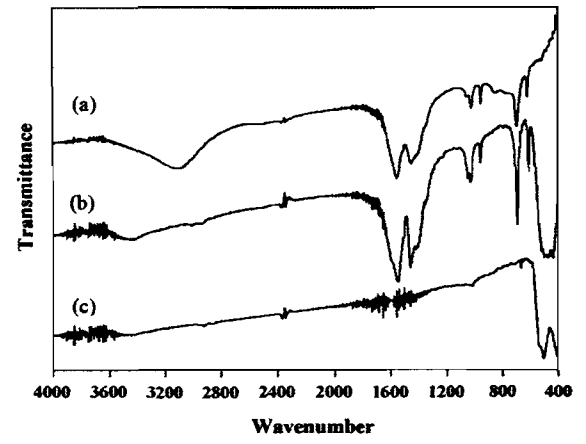


Fig. 7. IR spectra of: (a) the reaction precursor, i.e. zinc acetate, (b) ZnO synthesized in 1-octanol at 150 °C and (c) ZnO synthesized in 1-octanol at 200 °C.

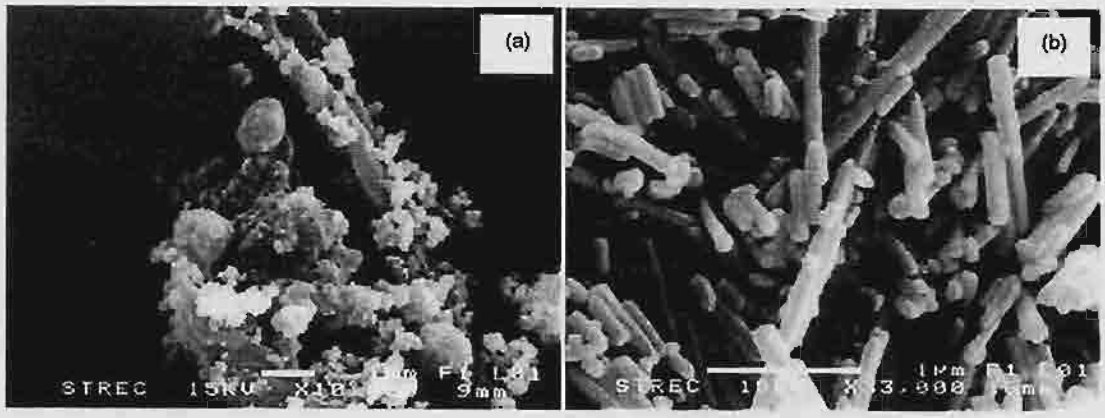


Fig. 8. SEM images of ZnO synthesized in 1-octanol for 2 h at (a) 150 °C and (b) 250 °C.

growth from any particular face was controlled by a combination of internal factors (e.g. intermolecular bonding preference or dislocation in crystal) and external factors (e.g. supersaturation condition, reaction temperature and type of solvent) [21]. ZnO in wurtzite structure is a polar crystal with (0 0 1) facet having higher-symmetry (C6v) than the other faces. Therefore, crystal growth along *c*-axis, or (0 0 1) direction, is a typical behavior observed from wurtzite ZnO. Nevertheless, Cheng and Samulski [4] have reported that the growth rate from each face of ZnO under the condition of hydrothermal synthesis is also controlled by properties of solvent that affected the interface–solvent interactions. The results in this work supported this report. It was found that the aspect ratio of the ZnO product was correlated with physical properties of the solvent. Fig. 5 shows a plot between boiling points of solvent and aspect ratio of the ZnO product. Interestingly, a linear relationship was observed. Although direct relationship between the boiling point of solvent and the preferential crystal growth may not have scientifically significance, the boiling point of alcohol could be used as an index for "non-polar" nature of alcohol molecule. For all alcohols investigated, the hydrogen bonding and the dipole–dipole interactions among molecules are roughly the same, but the van der Waals dispersion forces are stronger in alcohol with longer hydrocarbon chain and it results in an increase in boiling point of alcohol. As the long-chain alcohol was employed as the reaction medium, the interaction between the alcohol molecules and the (0 0 1) facet of the ZnO crystal, which was the slight positively charged Zn surface, was weak, allowing ZnO crystal to grow along the preferential *c*-axis.

Although the crystallization phenomenon of ZnO nanorod is unambiguously demonstrated by the presented correlation shown in Fig. 5, the detailed mechanism of the crystal growth is still under investigation. However, the behavior shown in Fig. 5 should prove useful in practical application, since the correlation allows and estimation of the aspect ratio of ZnO nanorod from type of alcohol used.

### 3.2. *Investigation of reaction mechanism*

To understand the reaction mechanism, the reaction temperature in octanol was decreased to 200 and 150 °C, respectively. Fig. 6 shows the XRD patterns of thus-obtained products. It was found that the powder prepared at 150 °C was a mixture of zinc acetate and zinc oxide. No shift in XRD pattern was observed. IR spectra of the product as shown in Fig. 7 also confirmed the existence of zinc acetate in the product synthesized at 150 °C without the presence of functional groups corresponding to alcohol. These results indicated that no intermediate was formed from the reaction between zinc acetate and alcohol.

Fig. 8 shows SEM images of the as-synthesized products prepared at various temperatures. The product prepared at 150 °C was composed of two types of particles, i.e. the particles with irregular shape, which was assigned to be zinc acetate and rod-shaped particles of ZnO. The elemental mapping showed that carbon atoms were distributed only on the irregular-shaped particles. The content of carbon decreased dramatically at the boundary between the irregular-shaped particles and rod-like particles. This SEM observation, together with XRD and FTIR results, indicated that ZnO rods grew from the ZnO seeds formed via the direct decomposition of zinc acetate.

To further investigate the reaction mechanism, the solvent recovered after the reaction was collected and analyzed by gas chromatography. Ester and water were detected in the remaining solvent. Therefore, it was proposed that the interaction between zinc acetate and alcohol under the solvothermal conditions resulted in esterifaction reaction, which proceeded to form ZnO, ester and water, according to the following reaction:

$$Zn(CH_3COO)_2 + 2R\text{-}OH \rightarrow ZnO + 2CH_3\text{-}CO\text{-}R + H_2O$$

Once the ZnO seeds were formed, further reaction resulted in crystal growth of ZnO nanoparticles. The size and shape of the particles were controlled by the reaction condition, as discussed previously.

## 4. Conclusion

Zinc oxide nanorods were successfully prepared by one-step solvothermal reaction of zinc acetate in alcohols. The as-synthesized ZnO was found to be an aggregation of nanorods having aspect ratios of 1.7, 3, 4 and 5.6 when 1-butanol, 1-

Please cite this article in press as: P. Tonto et al., Preparation of ZnO nanorod by solvothermal reaction of zinc acetate in various alcohols, Ceram. Int. (2006), doi:10.1016/j.ceramint.2006.08.003

hexanol, 1-octanol and 1-decanol, respectively, was used as the reaction medium. The interesting linear relationship between boiling point of the solvent used and aspect ratio of the product obtained was observed. This plot can be used to select the appropriate solvent for the preparation of zinc oxide nanorod with desired aspect ratio.

## Acknowledgement

Authors would like to thank Thailand Research Fund and Commissions on Higher Education, Ministry of Education, Thailand for financial support.

## Reference

[1] Z.W. Pan, Z.R. Dai, Z.L. Wang, Nanobelts of semiconducting oxides, Science 291 (2001) 1947–1949.
[2] L. Guo, Y.L. Ji, H. Xu, Regularly shaped, single-crystalline ZnO nanorods with wurtzite structure, J. Am. Chem. Soc. Commun. 124 (2002) 14864–14865.
[3] Q. Li, V. Kumar, Y. Li, H. Zhang, T.J. Marks, R.P.H. Chang, Fabrication of ZnO nanorods and nanotubes in aqueous solutions, J. Am. Chem. Soc. 17 (5) (2005) 1001–1006.
[4] B. Cheng, E.T. Samulski, Hydrothermal synthesis of one-dimensional ZnO nanostructures with different aspect ratios, Chem. Commun. (2004) 986–987.
[5] H. Wei, Y. Wu, N. Lun, C. Hu, Hydrothermal synthesis and characterization of ZnO nanorods, Mater. Sci. Eng. A 393 (2005) 80–82.
[6] Y Yang, H. Chen, Size control of ZnO nanoparticles via thermal decomposition of zinc acetate coated on organic additives, J. Cryst. Growth 263 (2004) 447–453.
[7] P. Saravanan, S. Alam, G.N. Mathur, Synthesis of ZnO and ZnS nanocrystals by thermal decomposition of zinc (II) cupferron complex, Mater. Lett. 58 (2004) 3528–3531.
[8] M.N. Kamalasanan, S. Chandra, Sol–gel synthesis of ZnO thin films, Thin Solid Films 288 (1996) 112–115.
[9] R. Mueller, L. Mädler, S.E. Pratsinis, Nanoparticle synthesis at high production rates by flame spray pyrolysis, Chem. Eng. Sci. 58 (2003) 1969–1976.
[10] J.E. Rodriguez, A.C. Caballero, Controlled precipitation methods: formation mechanism of ZnO nanoparticles, J. Eur. Ceram. Soc. 21 (2001) 925–930.
[11] Y. Zhang, Y. Dai, Y. Huang, C. Zhou, Shape controlled synthesis and growth mechanism of one-dimensional zinc oxide nanomaterials, J. Univ. Sci. Technol. Beijing 11 (2004) 23–29.
[12] J.Y. Li, X.L. Chen, H. Li, M. He, Z.Y. Qiao, Fabrication of zinc oxide nanorods, J. Cryst. Growth 233 (2001) 5–7.
[13] K. Sue, K. Kimura, M. Yamamoto, K. Arai, Rapid hydrothermal synthesis of ZnO nanorods without organics, Mater. Lett. 58 (2004) 3350–3352.
[14] J.Q. Hu, X.L. Ma, Z.Y. Xie, N.B. Wong, C.S. Lee, S.T. Lee, Characterization of zinc oxide crystal whiskers grown by thermal evaporation, Chem. Phys. Lett. 344 (2001) 97–100.
[15] Y. Liu, Z. Liu, G. Wang, Synthesis and characterization of ZnO nanorods, J. Cryst. Growth 252 (2003) 213–218.
[16] S.C. Lyu, Y. Zhang, H. Ruh, H.J. Lee, H.W. Shim, E.K. Suh, C.J. Lee, Low temperature growth and photoluminescence of well-aligned zinc oxide nanowires, Chem. Phys. Lett. 363 (2002) 134–138.
[17] X. HaiYan, W. Hao, Hydrothermal synthesis of zinc oxide powders with controllable morphology, Ceram. Int. 30 (2004) 93–97.
[18] O. Mekasuwandumrong, H. Kominami, P. Praserthdam, M. Inoue, Synthesis of thermally stable x-alumina by thermal decomposition of aluminum isopropoxide in toluene, J. Am. Ceram. Soc. 87 (2004) 1543–1549.
[19] S. Iwamoto, K. Saito, M. Inoue, K. Kagawa, Preparation of the xerogels of nanocrystalline titanias by the removal of the glycol at the reaction temperature after the glycothermal method and their enhanced photocatalytic activities, Nano Lett. 1 (2001) 417–421.
[20] M. Inoue, H. Kominami, T. Inui, Novel synthesis method for thermally stable monoclinic zirconia. Hydrolysis of zirconium alkoxides at high temperatures with a limited amount of water dissolved in inert organic solvent from the gas phase, App. Catal. A Gen. 121 (1995) L1–L5.
[21] N. Kubota, Effect of impurities on the growth kinetics of crystals, Cryst. Res. Technol. 36 (2001) 749–769.

# Effect of Aging on Synthesis of Graft Copolymer of EPDM and Styrene (EPDM-*g*-PS)

**Chalermpol Wonglert, Supakanok Thongyai, Piyasan Praserthdam**

*Center of Excellence on Catalysis and Catalytic Reaction Engineering, Department of Chemical Engineering, Chulalongkorn University, Bangkok 10330 Thailand*

Received 30 September 2004; accepted 14 March 2006
DOI 10.1002/app.24673
Published online in Wiley InterScience (www.interscience.wiley.com).

**ABSTRACT:** The effect of aging on synthesis by the graft copolymerization of styrene onto random ethylene–propylene–diene monomer with benzoyl peroxide (BPO) as the initiator is described. Results showed that yields of graft copolymer are increased in the first 10 min. After 10 min, the total polymer produced has a maximum at about 25 min. However, the portion of the graft copolymer is decreased and the portion of the pure polystyrene is increased. In addition, the influence factors, such as reaction time, temperature, BPO concentrations and styrene concentrations, effect of solvents on the extent of graft copolymerization were discussed. The extent of grafted copolymerization was verified by hexane and acetone Soxhlet (solvent extraction). © 2006 Wiley Periodicals, Inc. J Appl Polym Sci 102: 4809–4813, 2006

**Key words:** EPDM/styrene graft copolymer; benzoyl peroxide; aging effect

## INTRODUCTION

Graft copolymer of styrene (St) with ethylene–propylene–diene monomer (EPDM) has been widely studied in recent years. Among the several attempts to improve the weak points of high impact polystyrene (HIPS), the substitution of EPDM for butadiene has been widely investigated.[1,2] The usual method is to replace the butadiene with EPDM because it has long been known that EPDM has outstanding resistance[3] to heat, light, oxygen, and ozone because of its nonconjugated diene component.[4] In this study, St monomers were grafted onto EPDM under argon atmosphere in the presence of benzoyl peroxide (BPO) as an initiator. Various variables were observed to maximize the yield of product copolymer, such as aging of the solution, the concentration of St and others. The previous BPO reaction on EPDM and St monomer has been preliminary studied.[5] However, effects of aging the solution before mixing with St has not been mentioned earlier, which could further increase the yield of the copolymer. The excellent properties of the copolymer are that the EPDM-*g*-PS has a good miscibility between blends with PS[6] than the normal EPDM and can be distributed in small domain size.[7]

The effects of the reaction time, temperature, initiator concentration, solvents, and aging time on the graft reaction were investigated. The yields of graft copolymer were analyzed by hexane Soxhlet and acetone Soxhlet. The hexane will dissolve EPDM or the short branch chain of EPDM-*g*-PS, while acetone will dissolve the polystyrene formed.[7]

*Correspondence to:* S. Thongyai (tsupakan@chula.ac.th).
Contract grant sponsors: Thailand Research Fund (TRF); TJTTP-J.




## EXPERIMENTAL

### Materials

The Dupont EPDM 4640 rubber used was donated by S.K. Polymer Co., Thailand. The St monomer used to prepare the copolymer was manufactured by Fluka Chemie A.G., Switzerland, and purified with NaOH and distilled under vacuum before use. The BPO, as a free radical initiator, was manufactured by Merck, Muchen, Germany, and recrystallined in ethanol before use. The solvents such as *n*-hexane, heptane, THF, and toluene were of analytical purity and used as received.

### Preparation

EPDM (~ 5 g) was dissolved in 50 mL of toluene and heated at 80°C. The solution was stirred until the EPDM was completely dissolved. Free radical initiator used was BPO, which was recrystallined in ethanol to remove the impurities. St monomer was extracted with NaOH solution (5% w/w) in distillated water, and then was further purified by distilling over sodium under vacuum atmosphere before use.

### Graft copolymer polymerization

The copolymerization was conducted in a 250-mL three-neck flask equipped with stirrer, under argon

atmosphere. The graft reaction was carried out in toluene solvent at 60 or 90°C. To stop the polymerization reaction, excess acidic methanol was added to the reaction solution. The precipitated polymer was washed with methanol and dried under vacuum. The unreacted EPDM was extracted in hexane Soxhlet extractor and the produced polystyrene was further extracted in acetone Soxhlet extractor[8] for 12 h and the remaining graft copolymer of EPDM and St (EPDM-*g*-St) was obtained after drying.

## RESULTS AND DISCUSSION

The purpose of this work is to limit the optimum condition in the synthesis of graft copolymer of EPDM and polystyrene to improve the properties of the obtained polymer blends. Therefore, this section provides information about some preliminary results concerning the reaction conditions such as polymerization time, polymerization temperature, concentration of initiator, condition of synthesis, effect of solvent as a synthesis medium, and effect of aging for initializing the synthesis. The characterizations of graft copolymer were conducted by NMR and DSC.[7] Moreover, the tensile strength tests have been used to investigate the mechanical properties reported elsewhere.[7]

### Effect of time on synthesis of graft copolymer of EPDM and St

The effect of reaction time was investigated by varying the time for polymerization of EPDM and St in the range of 1–4 h while using BPO as the initiator. The copolymerization was performed in toluene at 90°C using ~ 5 g of EPDM, $1.50 \times 10^{-3}$ to $2.08 \times 10^{-3}$ mol/L BPO concentration, with total St concentration of 2.49 mol/L. The influence of time on the synthesis of graft copolymer is shown in Figure 1.

From the previous data of Sheng,[5] the yield of the copolymer will increase as time goes by and slightly increase after 1 h of polymerization. In a trend similar to that in Sheng's work, the copolymer formed (after extracting with acetone) has the tendency to saturate at certain yield. However, when the polymerization time reaches 4 h, the portion that did not dissolve in acetone (the moderate branch EDPM-*g*-PS) starts to increase abruptly, which indicated that the growth of the side chains exceeds the solubility limit in hexane (EDPM and short branch EDPM-*g*-PS will dissolve in hexane), while the quantity of PS formed (that dissolved in acetone) is quite constant. The experiments ceased after 4 h because the activity of the catalytic process are not worth to perform. The difference between Sheng's data and our data is the properties of the EDPM and reaction conditions used, which might lead to different results; but, however the tendency of the graph is very similar.

### Effect of BPO initiator concentration on the synthesis of graft copolymer of EPDM and St

The effects of the initiator concentration were investigated under 3 h polymerization times. The concentration of BPO initiator was varied in the range of $2.08 \times 10^{-3}$ to $6.25 \times 10^{-3}$ mol/L. The polymerizations were performed in toluene at 90°C using ~ 5 g of EPDM, with St concentration of 2.49 mol/L. The influence of BPO concentration on synthesis of graft copolymer is shown in Figure 2.

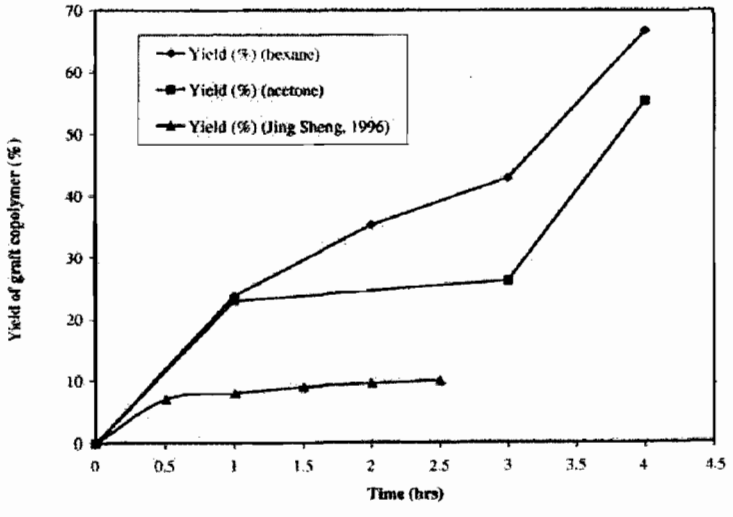


Figure 1 Yield of graft copolymer at different times. Polymerization conditions: EPDM, 3–5 g; [St], 2.49 mol/L (20 mL); BPO, $1.50 \times 10^{-3}$ to $2.08 \times 10^{-3}$ mol/L; solvent, toluene; polymerization temperature, 90°C.

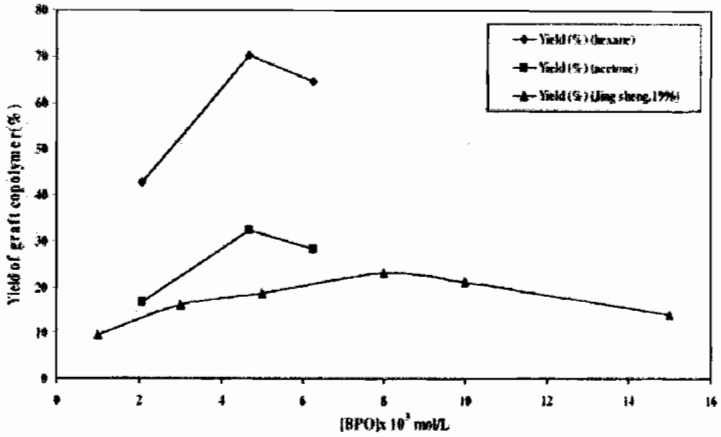


**Figure 2** Yield of graft copolymer at different BPO concentrations. Polymerization conditions: EPDM, 5.687 g; [St], 2.49 mol/L (20 mL); time, 3 h; solvent, toluene; polymerization temperature, 90°C.

As shown in Figure 2, the yield of the synthesized graft copolymer increased with increasing concentrations of BPO, leading to a maximum value at about $4.67 \times 10^{-3}$ mol/L. When the percent of BPO was less than the maximum value, the amounts of monomer radical, polymer radical, and graft copolymer radical increased with increasing concentrations of BPO, which increased the probability of interaction of radicals. When the percent of BPO was in excess, the grafting percent of St onto EPDM was decreased because the reaction of BPO by itself gradually increases. The viscosity of polymerization was increased with synthesis time, and because of the increasing concentration of BPO, which was evident, the movement of radicals was more difficult.[5] The trend of the results can be compared with Sheng's, but the differences arise due to the dissimilar reaction conditions. (In Sheng's work, concentration of EPDM was 60 g/L, St concentration was 0.3 mol/L, and time of reaction was 2 h.)

### Effect of solvents on synthesis of graft copolymer of EPDM and St

The effects of solvents were investigated by using polymerization time of 1 h. The temperature for polymerization of EPDM and St was 60 and 90°C. The polymerizations were performed using ~ 5 g of EPDM, $1.507 \times 10^{-3}$ to $2.039 \times 10^{-3}$ mol/L BPO concentrations, with total St concentration of 1.24 mol/L. The influences of solvent on synthesis of graft copolymer are shown in Table I for the reaction at 60°C and in Table II for the reaction at 90°C.

As shown in Table I, at 60°C, yields of graft copolymer were increasing from THF, hexane, toluene, and heptane respectively. However, at the temperature of 90°C, toluene gave more yield than heptane and eight times higher yield from the same solvent at 60°C (Table I). The nature of solvent may also affect $k_d$ (rate of thermal decomposition).[9] Therefore, rate of thermal decomposition of BPO to give free radical depends on various solvents and temperature, as can be seen. Therefore, at temperature of 90°C, cyclic solvent gives higher initiator radical than linear solvent in the process of high grafting polymer.

**TABLE I**
**Yield of Graft Copolymer of Each Solvent at 60°C**

| Solvent | Yield (%) (hexane) | Activity (g of polymer/(mol of BPO) h |
|---|---|---|
| Toluene | 1.65 | 147.83 |
| Hexane | 0.24 | 21.357 |
| Heptane | 2.71 | 203.25 |
| THF | 0.03 | 2.72 |

Polymerization conditions: EPDM, 4–5 g, [St], 1.24 mol/L (10 ml); BPO, $1.507 \times 10^{-3}$ to $2.039 \times 10^{-3}$ mol/L; polymerization temperature, 60°C.

### Effect of temperatures on the synthesis of graft copolymer of EPDM and St in toluene solvent

The effect of temperature was investigated by using BPO concentrations of $1.507 \times 10^{-3}$ and $2.039 \times 10^{-3}$ mol/L at 1 h for polymerization of EPDM and St. The polymerizations were performed in toluene and using ~ 5 g of EPDM and 1.24 mol/L concentration

**TABLE II**
**Yield of Graft Copolymer of Each Solvent at 90°C**

| Solvent | Yield (%) (hexane) | Activity (g of polymer/(mol of BPO) h) |
|---|---|---|
| Heptane | 25.57 | 1915.76 |
| Toluene | 29.30 | 2192.96 |

Polymerization conditions: EPDM, 4–5 g, [St], 1.24 mol/L (10 ml); BPO, $1.507 \times 10^{-3}$ to $2.039 \times 10^{-3}$ mol/L; polymerization temperature, 90°C.

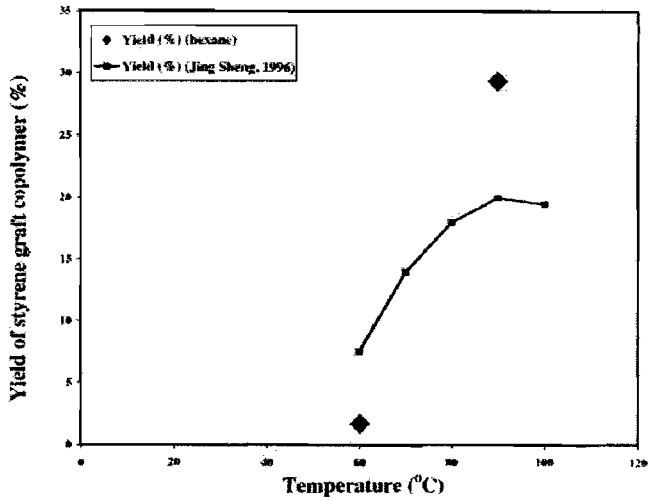


**Figure 3** Yield of graft copolymer at different temperatures. Polymerization conditions: EPDM, 4–5 g; [St], 1.24 mol/L (10 mL), BPO, $1.507 \times 10^{-3}$ to $2.039 \times 10^{-3}$ mol/L; solvent, toluene.

of St. The influence of temperature on synthesis of graft copolymer is shown in Figure 3.

As shown in Figure 3, yield of graft copolymer increased with increasing temperature, yielding a maximum value at 90°C and then decreased at the same time, presumably because of the reduction of the half-life of BPO with rising temperature,[10] which would increase the number of BPO radicals. When the temperature of the reaction was more than 90°C, the extent of grafting decreased because the number of radicals was decreased while increasing velocity of decomposition of BPO.[5] Thus, most of the reactions are commenced at 90°C.

### Effect of aging time on synthesis of graft copolymer of EPDM and St

The effect of aging time was investigated by using BPO as the initiator. The time for polymerization of EPDM and St was set at 2 h. The copolymerization was performed in toluene at 90°C using ~ 5 g of EPDM, BPO concentration about $1.50 \times 10^{-3}$ to $2.08 \times 10^{-3}$ mol/L,

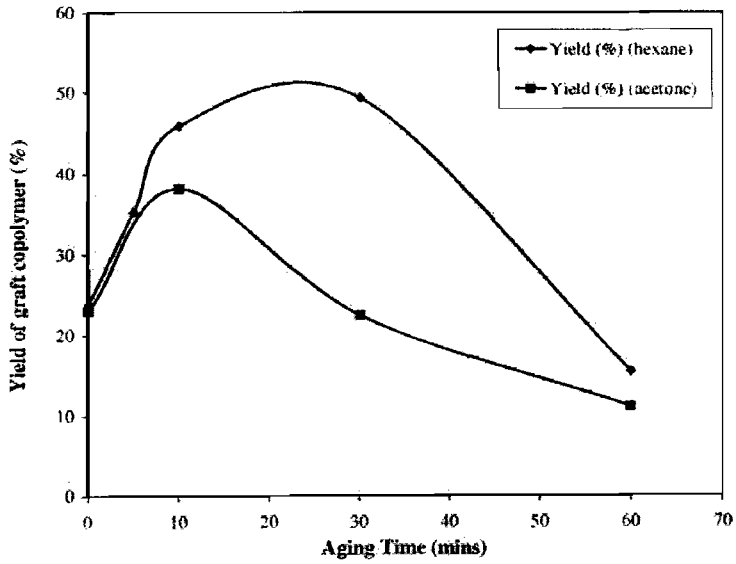


**Figure 4** Yield of graft copolymer at different aging times. Polymerization conditions: EPDM, 3–5 g; BPO, $1.5 \times 10^{-3}$ to $2.08 \times 10^{-3}$ mol/L; solvent, toluene; polymerization temperature, 90°C; polymerization time, 2 h.

with total St concentration of 2.49 mol/L. The influence of aging time on synthesis of graft copolymer is shown in Figure 4.

As shown in Figure 4, yield of graft copolymer increased with increasing aging time, yielding a maximum value at 10 min (acetone) and 30 min (hexane). After 10 min, the portion that can be dissolved in acetone is increased, which indicates that more polystyrene is formed and can be detected by the portion that dissolved in acetone. However, the aging time is important for the reaction because the initial reaction solutions were very viscous and the reaction of the free radical is impeded by the viscosity of the solution. However, the BPO free radical can be decomposed by as many processes[7] and too long aging may cause adverse effects on the reactions, which can be clearly seen in Figure 4.

## CONCLUSIONS

This research revealed the importance of aging time besides all the process parameters. The increase of the aging time to an appropriate amount will increase the yield of EPDM-g-PS to a larger extent. However, too much aging time will cause adverse effect on the polymerization reaction. All the process parameters were elucidated, which also comply with the results of Sheng.[5] Effect of solvents at different temperatures were stated, and in this reaction, toluene is the best solvent.

## References

1. Meredith, C. L.; Von Bodungen, G. A. U.S. Pat. 3,657,395 (1972).
2. Shimokawa, S.; Yamamoto, Y. U.S. Pat. 4,314,041 (1982).
3. Crevecoeur, J. J.; Nelissen, L.; van der Sanden, M. C. M.; Leinstra, P. J. Polymer 1995, 36, 753.
4. Qu, X.; Shang, S.; Lin, C.; Zhang, L. J Appl Polym Sci 2002, 86, 428.
5. Sheng, J.; Hu, J. J Appl Polym Sci 1996, 60, 1499.
6. Sheng, J.; Hu, J.; Yuan, X.-B.; Han, Y.-P.; Li, F.-K.; Bian, D.-C. J Appl Polym Sci 1998, 70, 805.
7. Wonglert, C. M.S. Thesis, Chulalongkorn University, Thailand, 2003.
8. Chung, T. C.; Janvikul, W.; Bernard, R.; Jaing, G. J. Macromolecules 1994, 27, 26.
9. Matyjazewski, K.; Thomas, D. P. Handbook of Radical Polymerization; Wiley: New York, 1998.
10. Stevens, M. P. Polymer Chemistry: An Introduction, 3rd ed.; Oxford University Press: New York, 1999.

# New Synthesis Methods for Polypropylene-*co*-Ethylene-Propylene Rubber

**Satit Thanyaprueksanon, Supakanok Thongyai, Piyasan Praserthdam**

*Department of Chemical Engineering, Center of Excellence on Catalysis and Catalytic Reaction Engineering, Faculty of Engineering, Chulalongkorn University, Bangkok 10330 Thailand*

Received 8 May 2006; accepted 13 August 2006
DOI 10.1002/app.25392
Published online in Wiley InterScience (www.interscience.wiley.com).

**ABSTRACT:** In this research, the reinforcement of polypropylene (PP) was studied using a new method that is more practical for synthesizing polypropylene-*block*-poly(ethylene-propylene) copolymer (PP-*co*-EP), which can be used as a rubber toughening agent. This copolymer (PP-*co*-EP) could be synthesized by varying the feed condition and changing the feed gas in the batch reactor system using Ziegler–Natta catalysts system at a copolymerization temperature of 10°C. The $^{13}$C-NMR tested by a 21.61-ppm resonance peak indicated the incorporation of ethylene to propylene chains that could build up the microstructure of the block copolymer chain. Differential scanning calorimetry (DSC), scanning electron microscopy (SEM), and dynamic mechanical analysis (DMA) results also confirmed these conclusions. Under these conditions, the morphology of copolymer trapped i PP matrix could be observed and the copolymer $T_g$ woul decrease when the amount of PP-*co*-EP was increased. DM study also showed that PP-*co*-EP is good for the polypropy ene reinforcement at low temperature. Moreover, the PP-*c* EP content has an effect on the crystallinity and morpholog of polymer blend, i.e., the crystallinity of polymer decrease when the PP-*co*-EP content increased, but tougher mechan cal properties at low temperature were observed. © 200 Wiley Periodicals, Inc. J Appl Polym Sci 103: 3609–3616, 2007

**Key words:** polypropylene-*co*-poly(ethylene-propylene copolymer; synthesis; rubber toughening; Ziegler–Natt polypropylene

## INTRODUCTION

Isotactic polypropylene (iPP) is a typical semi-crystalline polymer that has been used to produce various products. However, it has a mechanical properties limit. It is well known that iPP has poor mechanical properties in the low-temperature range (0°C in the normal refrigerator) under its glass transition temperature ($T_g$). The general method to improve the mechanical properties of iPP is to blend iPP with a rubbery material such as poly(ethylene-propylene), copolymer (EPR), ethylene-propylene-diene terpolymer (EPDM), or any other copolymer.[1–3] The iPP/EPR blends, called toughened polypropylene, have been widely used in consumer products and automotive industry. However, the strong incompatibility of EPR and iPP has presented a considerable problem in the modification of mechanical properties of iPP/EPR blending systems/methods.[4]

Copolymers are interesting alternatives as important materials to improve mechanical properties of iPP. The propylene-*co*-poly(ethylene-propylene) copolymer is one of the polymers that can be used for the rubber toughening of PP. Examples of the syntheses and characterization of PP-*co*-EP have bee reported.[5–11]

Coates and colleagues[5] reported the synthesis of syndiotactic polypropylene-*block*-poly(ethylene-pro pylene) with a metallocene catalyst system. Fukui an Murata[6] also reported the synthesis of polypropylene *block*-poly(ethylene-*co*-propylene), using metallocen catalyst systems. However, these catalysts are n only expensive but are also rapidly deactivated b moisture and oxygen. Until now, the metallocen catalysts have remained difficult to operate and us practically.

Nitta et al.[7] reported that the PP/EPR blends an polypropylene-*block*-poly(ethylene-*co*-propylene) ca be synthesized by a short-period polymerizatio method. Mori et al.[8] reported the synthesis of a poly propylene-*block*-poly(ethylene-propylene) by high pressure-type and stopped-flow polymerization meth ods using the Ziegler–Natta catalyst.

However, the short-period polymerization an stopped-flow polymerization methods are not practi cal and are too complicated in polymer synthesis fields as they must be controlled by a computer to generat sudden changes in gas feed conditions in 0.2 s.

Fan et al.[9] reported that fraction of structure an properties of iPP/EPR in situ blend was synthesize by spherical Ziegler–Natta catalyst in two stages: th liquid phase propylene homopolymerization, and the the gas phase ethylene-propylene copolymerization.

*Correspondence to:* S. Thongyai (tsupakan@chula.ac.th).

However, all the above-mentioned methods are not practical to use in the industrial applications. To overcome the problem, this work presents a new and simple method for the synthesis of polypropylene-*co*-poly (ethylene-propylene) (PP-*co*-EP) copolymer, using the Ziegler–Natta catalyst for industrial production. The nuclear magnetic resonance (NMR) results confirmed the corporation of ethylene (E) in the molecule of propylene (P). The results of differential scanning calorimetry (DSC) and dynamic mechanical analysis (DMA) show that less pure P and pure E are produced in the PP-*co*-EP polymers. The copolymer obtained can be used for the rubber toughening of polypropylene. The DMA results show the advantage in the low temperature range below $T_g$ of the pure PP in the blending of PP with PP-*co*-EP polymers.

## EXPERIMENTAL

### Materials

Ethylene and propylene (polymerization grade) and triethylaluminum ($AlEt_3$; TEA) were obtained from Bangkok Polyethylene Company (Bangkok, Thailand). $TiCl_4$ was purchased from Merck. Anhydrous $MgCl_2$ was supplied by Sigma-Aldrich; phthalic anhydride, diethylphthalate (DEP, used as an internal donor) and *n*-decane were purchased from Fluka Chemie A.G. (St. Gallen, Switzerland). Hexane was donated by Exxon Chemical Thailand (Bangkok, Thailand).

The solvents were distilled over sodium/benzophenone under argon atmosphere before use. Ultra-high-purity (UHP) argon (99.999%) was obtained from Thai Industrial Gas Company (Bangkok, Thailand) and was further purified by molecular sieves –3 Å, BASF catalyst R3-11G, NaOH, and phosphorus pentoxide ($P_2O_5$), to remove traces of oxygen and moisture. Commercial-grade polypropylene was donated by the Thai Polyplastic Industry Public Company (Bangkok, Thailand).

All chemicals were manipulated under purified argon. All operations were carried out under an inert atmosphere of argon, using a vacuum atmosphere glove box and/or standard Schlenk techniques.

### Preparation of catalyst

Anhydrous magnesium chloride ($MgCl_2$), *n*-decane, and 2-ethyl-1-hexanol were put into a Schlenk tube and heated to 130°C for 2 h under magnetic stirring and argon atmosphere. Then phthalic anhydride was introduced into the solution and stirred until $MgCl_2$ was completely dissolved. The resulting uniform solution was cooled to room temperature, and wholly dropped wise of titanium tetrachloride ($TiCl_4$), kept stirring at –20°C. The temperature was then raised to 110°C, and diethylphthalate was injected in. The mixture was maintained at this temperature for 2 h. After the 2-h reaction, the solid portion was collected from the reaction mixture and again suspended in 20 mL of titanium tetrachloride and reacted at 120°C for another 2 h. It was then collected and later washed with *n*-decane and *n*-hexane for 2 and 3 times, respectively. The resulting solid was next vacuum dry to form a powder in gray color which must to be stored under argon atmosphere.

### Synthesis of polypropylene-*co*-poly (ethylene-propylene) copolymer

Polymerization was carried out in a 100-mL stainless steel autoclave reactor with magnetic stirrer in hexane, using a $MgCl_2$/DEP/$TiCl_4$–TEA catalytic system. The polymer was synthesized in a two-stage reaction process. First, the solvent, co-catalyst, and catalyst

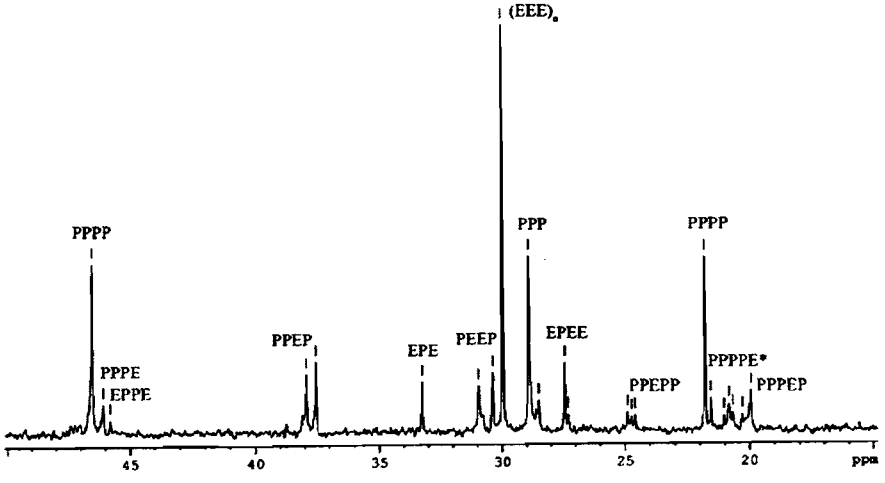


**Figure 1** $^{13}$C-NMR spectrum of PP-*co*-EP copolymer (polymer 5).

TABLE I
Characterization of Polymers by DSC

| Polymer[a] | Temp (°C) | $P_E$ (psi) | Mn | MWD | Heat 1[b] | | | Heat 2[b] | | | |
|---|---|---|---|---|---|---|---|---|---|---|---|
| | | | | | $T_g$ | $T_{m1}$ | $T_{m2}$ | $T_g$ | $T_{m1}$ | $T_{m2}$ | $T_c$ |
| Polymer 1 | 60 | 50 | — | — | −21.34 | nd | nd | −22.51 | 113.80 | 147.10 | 92.04 |
| Polymer 2 | 40 | 50 | — | — | −17.41 | 123.67 | 152.35 | −17.64 | 124.97 | 150.45 | 99.34 |
| Polymer 3 | 10 | 50 | — | — | −15.88 | 117.84 | 147.19 | −14.72 | 118.67 | 145.70 | 91.47 |
| Polymer 4 | 10 | 60 | — | — | −16.96 | 124.99 | 148.67 | −16.25 | 116.11 | 146.82 | 94.83 |
| Polymer 5 | 10 | 70 | 141,528 | 12.24 | −21.72 | 126.10 | 145.34 | −22.41 | 117.22 | 143.13 | 95.93 |
| Polymer 6 | 10 | — | 65,658 | 9.08 | −9.86 | nd | 151.25 | −10.85 | nd | 149.40 | 102.25 |

nd, not detected.
[a] Synthesis by $TiCl_4/MgCl_2$/DEP-TEA, Al/Ti = 167; propylene pressure feeding constant = 30 psi.
[b] Ramp rate = 40°C/min both heating and cooling; heating 1 – cooling – heating 2 from −60° to 200°C.

were added into the reactor, and subsequently placed in some liquid nitrogen to control the reaction between the catalyst and co-catalyst. After that, the reactor was evacuated to remove both the argon and the liquid nitrogen, and then heated up to polymerization temperature. The first stage of polymerization is the propylene homopolymerization, to feed only propylene gas into the reactor for 10 min. The reactor was then heated under the controlled temperature to start the polymerization reaction. The second stage is to copolymerize the ethylene into the PP structure by successively feeding the pure ethylene gas into a stirred reactor for a duration of 30 min. The mixture was then quenched in the HCl/methanol solution after the completion of the reaction. The polymer obtained that precipitates out is to be washed thoroughly in methanol and finally dried at room temperature.

### Blending and molding of polymer

Polypropylene (PP) and the PP-co-EP were combined by the melt-mixing method on a digital hot plate at 220°C whit 5%, 10%, 15%, and 20% of PP-co-EP. The polymer blend was then was molded with LAB TECH Automatic Hydraulic Hotpress LP-50 M/C 9701 in an aluminum mold at 200°C 1500 psi. Then, the polymer blend was cooled down at room temperature. The sample size for tensile testing is 20 × 100 × 0.5 mm and 10 × 40 × 0.5 for DMA.

### Characterization

DSC analyses of polymers were carried out using Perkin-Elmer Diamond DSC, calibrated for temperature and melting enthalpy, with indium as the standard. Each sample, ~ 10 mg in weight, was sealed in an aluminum pan for further measurement before being heated from −60 to 200°C at a scanning rate of 40°C/min under $N_2$ atmosphere.

$^{13}$C-NMR spectra of the polymers were measured on an Avance DPX400 NMR spectrometer at 120°C, while *o*-dichlorobenzene and benzene-$d_6$ were used as solvents to prepare the polymer solution.

The morphologies of all polymer fracture surfaces were investigated with a JSM-5410LV scanning electron microscope (SEM). The samples for SEM analysis

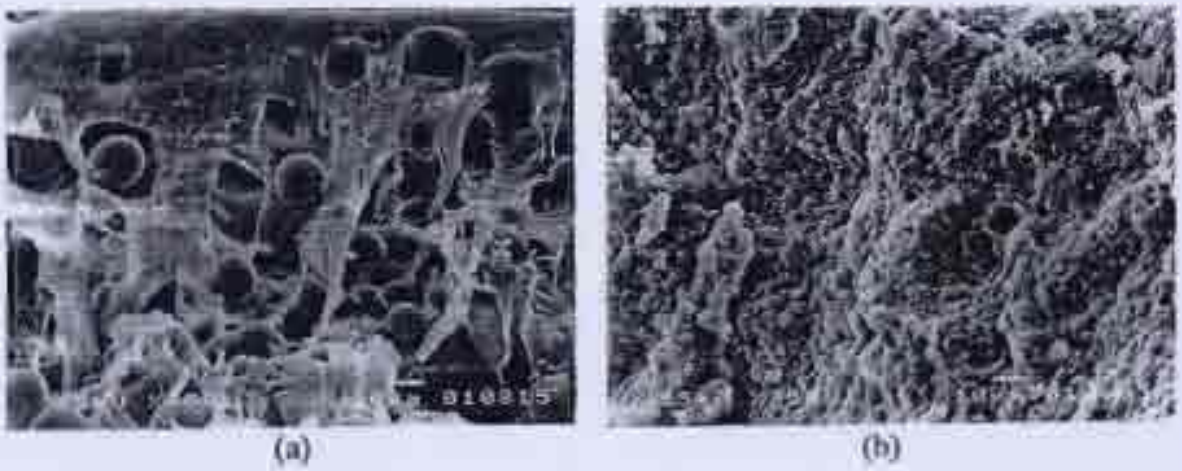

(a) (b)

Figure 2 SEMs of cryogenic polymer fracture surface. (a) Polymer fracture of PP-block-EP copolymer 5; (b) polymer fracture of PP (polymer 6). ×750.

**TABLE II**
**Characteristics of Polymer Blend and Polypropylene**

| | | | Heat 1[b] | | | Heat 2[b] | | | Cool[b] | |
|---|---|---|---|---|---|---|---|---|---|---|
| Polymer[a] | Mn | MWD | $T_g$ | $T_m$ | $\Delta H$ | $T_g$ | $T_m$ | $\Delta H$ | $T_c$ | $\Delta H$ |
| EP00 | 35,283 | 10.47 | −0.22 | 165.96 | 97.18 | −1.45 | 165.96 | 96.59 | 106.92 | 96.54 |
| EP05 | — | — | −7.48 | 167.07 | 95.76 | −8.42 | 165.21 | 94.03 | 109.08 | 95.61 |
| EP10 | 56,474 | 4.09 | −10.54 | 167.82 | 91.91 | −11.13 | 167.79 | 91.68 | 108.70 | 91.64 |
| EP15 | — | — | −13.98 | 166.31 | 89.13 | −14.82 | 165.21 | 88.69 | 109.75 | 88.88 |
| EP20 | 70,676 | 4.96 | −16.14 | 164.18 | 83.53 | −16.34 | 162.13 | 83.33 | 110.17 | 83.38 |

[a] EP00, EP05, EP10, EP15, and EP20, referring to PP, were added PP-*b*-EP 0%, 5%, 10%, 15%, and 20%, respectively.
[b] Ramp rate = 40°C/min both heating and cooling; heating 1 – cooling – heating 2 from −60° to 200°C, $\Delta H$ = kJ/g.

were coated with gold particles by ion sputtering device to provide electrical contact for the specimens.

Dynamic mechanical properties of blending polymers were characterized, using Perkin-Elmer DMA-Pyris Diamond. The entire experiment was operated at 1 Hz in tension mode over a temperature range of −140°C to 150°C with 1.5°C/min; sample sizes were 10 × 50 × 0.5 mm, using liquid nitrogen as the cryogenic medium.

The molecular weight and molecular weight distribution were finally determined using gel permeation chromatography (GPC, Waters 2000) with Styragel HT6E column at 135°C with 1,2,4-trichlorobenzene as the solvent.

## RESULTS AND DISCUSSION

### Synthesis of copolymer

Figure 1 shows a typical $^{13}$C-NMR spectrum of the synthesized PP-*co*-EP (polymer 5). The chemical shift assignments for $^{13}$C resonances are similar to those reported by Fukui et al.[6] The mole fractions of propylene/ethylene unit (P/E unit) in the block copolymer were determined as 37/63 mole% from the peak areas of methylene and methyl carbons.[12–15] From the $^{13}$C-NMR spectrum, the peak at 21.61 ppm showed the characteristic of propylene (P) that has the ethylene (E) laid in the adjacent of PPPPE, indicating the cooperation of E in the P chain. Because only the pure propylene was allowed in the reactor at the beginning, the first polymerization product in the reactor was the propylene pure chains only (for a duration of 10 min) The second step of polymerization allowed E to react in the reactor for a duration of 30 min, so that the discovered E incorporated in the P chain would support the formation of the block copolymer of PP and EP in the second stage. This shows that at least some of the PP chain will survive through the second stage of the reaction, with E incorporation as the consequence. Unfortunately, because of the batch reactions, the variation in the partial pressure of propylene and ethylene changed with time during the synthesis prevailed against the exact quantitative calculations of the cooperation of E in the P chain.

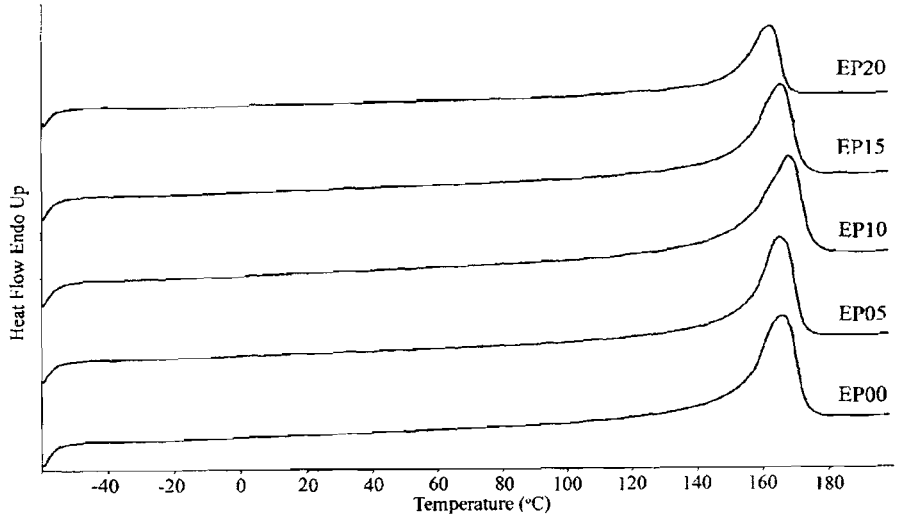


**Figure 3** DSC curves of EP00, EP05, EP10, EP15, and EP20.

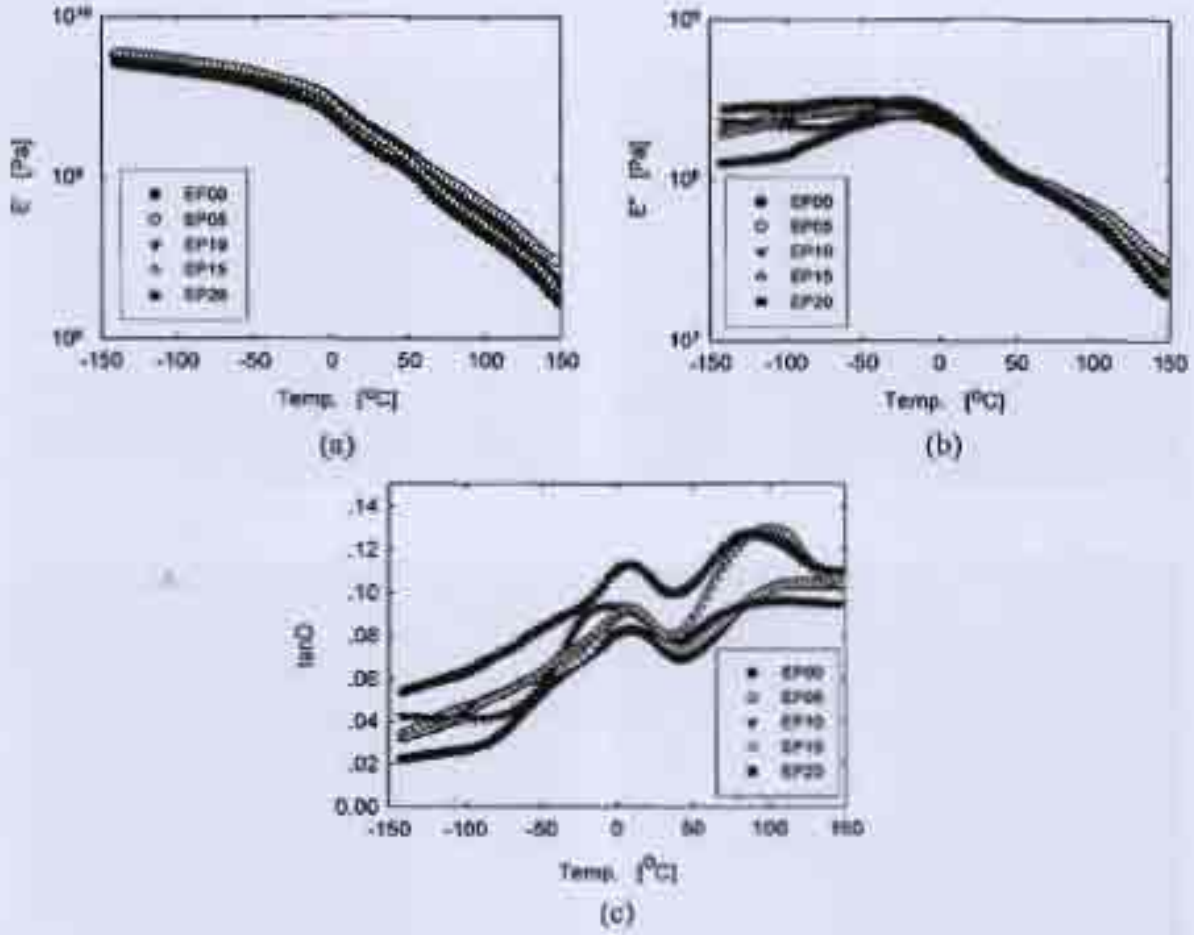


Figure 1 Temperature dependence of dynamic mechanical properties at 1 Hz. (a) Storage modulus; (b) loss modulus; (c) tanδ.

Table I shows the effects of polymerization temperature and pressure of corporate ethylene gas when added into the reactor at the glass transition temperature ($T_g$), melting temperature ($T_m$), and temperature of crystallization of PP-*co*-EP products from DSC results. In addition to the NMR result, the DSC graphs of $T_g$ of copolymer show that there are two phases in the PP-*b*-EP block copolymer, as the DSC results clearly show two $T_m$s in the synthesized polymers. In the first phase, PP is dominant and the other phase appears to have the E contribution.

From Table I we can conclude that a higher polymerization temperature gives the lower $T_g$ of the products. This might be because there is more incorporation of E in the P chain at the higher polymerization rate. Usually, the lower $T_g$ in the block copolymer will result from the incorporation of the low $T_g$ component (E) in the higher $T_g$ matrix (P). The lower $T_g$ also confirms the NMR results that E has cooperation in the PP chain without serious segregation of pure PP because no clear pure component $T_g$ of PP (−10–0°C) was detected. Moreover, synthesized polymers have the dispersed phase of the ethylene-propylene rubber even at the rector temperature of 60°C. Usually at higher temperature, polymerization will give results in the higher chain transfer rate (polymer 1, polymer 2, and polymer 3), which shorten the progressive chains of PP; it is most likely that the E cannot totally incorporate on the PP chain.

As a consequence, the higher feeding ethylene pressure gives the lower $T_g$ temperature (polymer 3, polymer 4, and polymer 5) at the same reaction temperatures. These may result from the higher incorporation of E, because the concentration of E is increased along with the pressure of the system. The higher concentration of E presented in the reactions shows the higher incorporation of E onto the PP chain and the samples. Unfortunately, with the limit of the DSC scanning temperature (from −60°C to 200°C), the $T_g$ of the pure E at −100°C was not confirmed. However, the lower

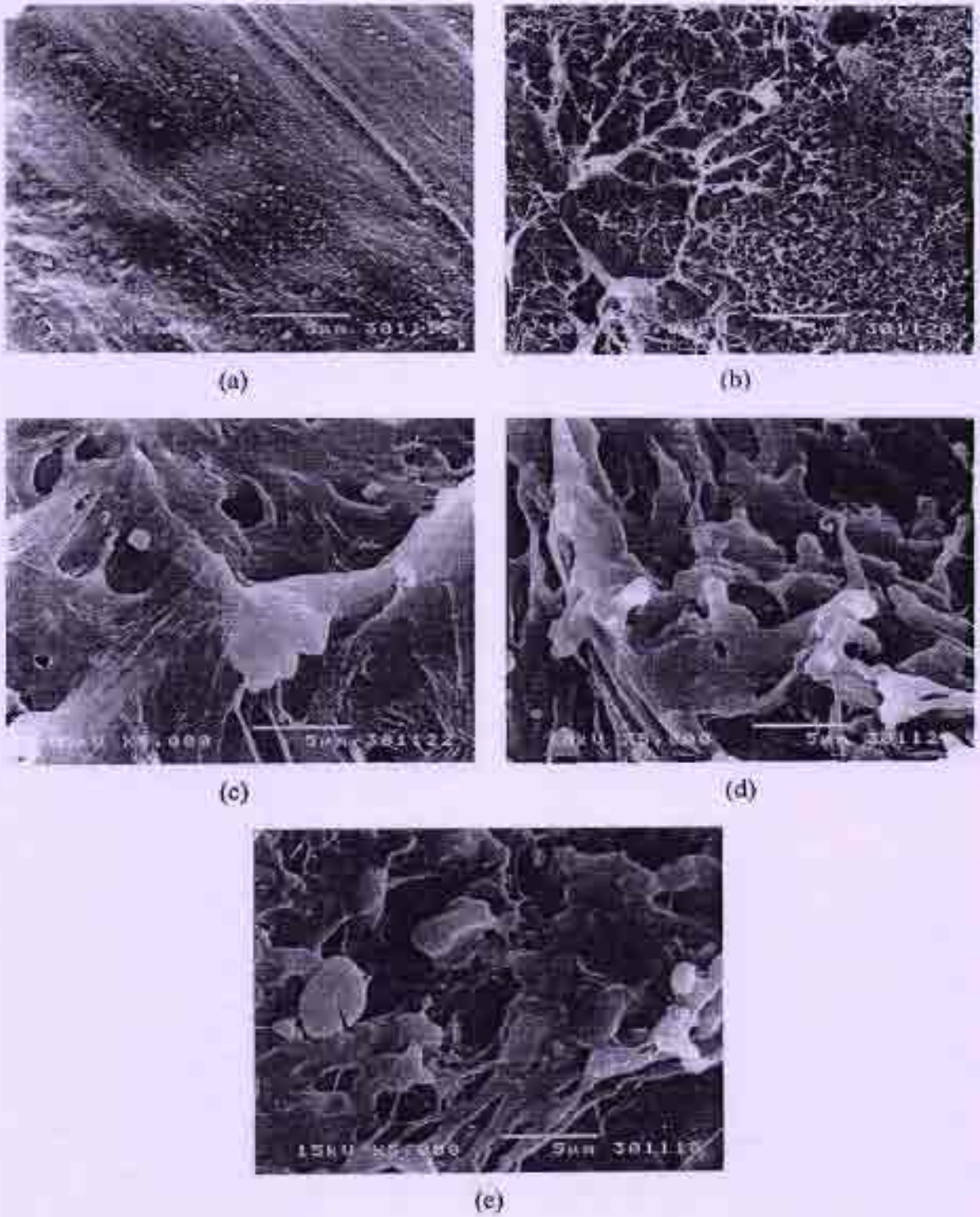

Figure 5 SEMs of room temperature specimen fracture. (a) EP00; (b) EP05; (c) EP10; (d) EP15; (e) EP20. ×5000.

$T_g$ of PP according to the incorporation of E in these systems also supports the incorporation of E onto PP chains without substantial termination of the active site of PP.

In polymer 6, only the P was allowed in the reactor, and the polymer formed is the PP only. Because the time for PP to react is the same as other samples before the supply of E to the reactor, the polymer formed will represent the PP chains before the cooperation of E. The clear $T_g$ of PP was observed at $-9$°C, which was clearly higher than the $T_g$ of the corporate polymer with E. The molecular weight of PP6 and the $T_m$ confirm the high quality of PP produced. If we further corporate E onto this PP, the polymer formed will have substantial characteristics of PP. Moreover, the higher $T_m$ of pure PP in polymer 6 than in the other cooperation of E samples shows that the crystals of pure PP were affected by the cooperation of E, and no clear separated peak $T_m$ for pure PP was observed again after cooperation with E.

According to the DSC results, the appearance of the rubbery phase of the block copolymer can be seen in SEMs of polymer fracture [Fig. 2(a)]) The minor phase of EP can be seen as the phase separated droplets in the fracture surface picture. In the pure PP micrographs [polymer 6, Fig. 2(b)], the droplet characteristics cannot be observed. These appearances support the DSC results that represent the two phase characteristics.

### Polymer blend

The influence of PP-*b*-EP incorporated in commercial-grade polypropylene on $T_g$, $T_m$, and $T_c$ of polymer blend is shown in Table II. The suffix number at the name of the blend stands for the weight percentage of the PP-*co*-EP added to the blend. As can be seen, $T_g$ value decreases with an increase of the PP-*b*-EP content (from 0% to 20%), while $T_m$ and $T_c$ values are not clearly affected. Generally, $T_g$ represents an amorphous part of polymer. The $T_g$ value of pure polypropylene is approximately 0°C (EP00) and the $T_g$ of the blend with PP-*co*-EP decreases with the increase of the PP-*b*-EP copolymer content.[7] The $T_g$ of polymer blend ranges from that of PP and synthesized PP-*b*-EP. The $T_m$ and $T_c$ results suggest that EP molecule does not substantially affect the crystallinity of polypropylene.[16] Moreover, $\Delta H$ indicated the crystallinity of polypropylene. It was found that $\Delta H$ decreased with an increase of PP-*b*-EP content. Thus, the addition of PP-*b*-EP can reduce the crystallinity of polypropylene.[17] Our results confirm the previous work on the blend of PP and EP;[7,16,17] thus, our PP-*co*-EP can affect the properties of the PP like other references but is better in that it has an easier preparation. Figure 3 shows heat 2 DSC curve of PP (EP00) and polymer blend in which the $T_m$ of the polymer blend was similar to PP.

Figure 4 shows the effect of PP-*b*-EP on the dynamic mechanical properties of the polymer blend. The result indicates that both PP and polymer blend have similar values of E within the range of $-140$–150°C [Fig. 4(a)]. As shown in Figure 3(b), the E of polymer blend is higher than PP at a temperature of $< 0$°C. This means that the polymer blend can dissipate more energy than pure polypropylene (EP00) at low temperature ($< 0$°C). Figure 4(c) shows the value of tan$\delta$, which is determined by $E''/E'$. The tan$\delta$ of polymer blend is higher than that of the pure polypropylene. It can be said that the toughness of the polymer blend increases within the range of low temperature, while PP-*co*-EP only presents in the polypropylene blend. In addition, the $T_\beta$ peak, ascribed to glass transition in amorphous part, is present in polymer blend [Fig. 4(c)]. The broader $T_\beta$ peak resulted from the incorporation of EP molecule in the amorphous PP region.[16] Moreover, the $T_g$ of E at $\sim -100$°C was not observed. This may suggest that the samples have too small an amount of PE molecules generated in amorphous phases to be detected by DMA.

As shown in Figure 5, SEM confirmed that the polymer blend has greater toughness than PP. From the room temperature fracture surface of polymer blends, these pictures show a rubbery morphology in addition to the PP matrix. The blends have an additional rubbery phase that stretches and binds the PP together. The more PP-*co*-EP added, the more the stretched rubbery phase can be observed. This rubbery phase might be responsible for the low-temperature toughness of the blends.

## CONCLUSION

The results presented show that the PP-*co*-EP can be synthesized by a simple method. The ethylene content in the copolymer chain increased while increasing the ethylene fed pressure. The $^{13}$C-NMR result indicated incorporation of ethylene in the propylene chain. DSC and SEM showed the rubbery material of the copolymer resulting from lowering the $T_g$ of the blends further than the $T_g$ of pure PP in the copolymers. The convenient condition shown in the present work for the synthesis PP-*co*-EP is 30 psi of propylene feeding and 70 psi of ethylene feeding pressure at a 10°C copolymerization temperature. The results of PP/PP-*b*-EP blends show a relationship among the PP-*b*-EP content with toughness, $T_g$, and crystallinity. DSC, DMA, and SEM indicated that the PP-*b*-EP included in the amorphous region of PP and the polymer blends have lower $T_g$ and crystallinity, but higher toughness, than commercial-grade PP within the low-temperature range. We can conclude that PP-*b*-EP is a

good rubber toughening agent for polypropylene reinforcement at low temperature that can be simply prepared, using the method described.

The authors thank the Bangkok Polyethylene Co. for supplying the ethylene and propylene gas, as well as the TEA and GPC characterization. We also thank the Thai Polyplastic Industry Public Co., Ltd., for its donation of the commercial-grade polypropylene. Furthermore, great appreciation is due to the MEKTEC Manufacturing Corporation (Thailand) Ltd., for its support of the equipment.

## References

1. Yokoyama, Y.; Ricco, T. Polymer 1998, 36, 3675.
2. Michler, G. H. In Polypropylene. An A–Z Reference; Karger-Kocsis, J., Ed.; Kluwer Academic: Dordrecht, the Netherlands, 1999; p 194.
3. Wang, Z. J Appl Polym Sci 1996, 60, 2239.
4. Teh, J. W.; Rudin, A.; Keung, J. C. Polym Technol 1994, 13, 1.
5. Tian, J.; Hustad, P. D.; Coates, G. W. J Am Chem Soc 2001, 123, 5134.
6. Fukui, Y.; Murata, M. Appl Catal A: Gen 2002, 237, 1.
7. Nitta, K.; Kawada, T.; Yamahiro, M.; Mori, H.; Terano, M Polymer 2001, 41, 6765.
8. Mori, H.; Yamahiro, M.; Prokhorov, V. V.; Nitta, K.; Terano, M Macromolecules 1999, 32, 6008.
9. Fan, Z.; Zhang, Y.; Xu, J.; Wang, H.; Feng, L. Polymer 2001, 42 5559.
10. Yamahiro, M.; Mori, H.; Nitta, K.; Terano, M. Polymer 1999 40, 5265.
11. Nitta, K.; Kawada, T.; Prokhorov, V. V.; Yamahiro, M.; Mori H. J Appl Polym Sci 1999, 74, 958.
12. Randall, J. C. Macromolecules 1978, 11, 33.
13. Randall, J. C. Macromol Chem Phys 1982, 29, 20.
14. Carman, C. J.; Harrington, R. A.; Wilkes, C. E. Macromolecules 1977, 10, 536.
15. Wang, W.; Zhu, S. Macromolecules 2000, 33, 1157.
16. Nitta, K.; Shin, Y.; Hashiguchi, H.; Tanimoto, S.; Terano, M Polymer 2005, 46, 965.
17. D'Orazio, L.; Mancarella, C.; Martuscelli, E.; Cecchin, G.; Corrieri, R. Polymer 1999, 40, 2745.
18. Liang, J. Z.; Li, R. K. Y. J Appl Polym Sci 2000, 77, 409.
19. Jang, B. Z.; Uhlmann, D. R.; Vander Sande, J. B. J Appl Polym Sci 1985, 30, 2485.
20. Tam, W. Y.; Cheung, T.; Li, R. K. Y. Polym Test 1996, 15, 363.

# Interfacial Adhesion Enhancement of Polyethylene–Polypropylene Mixtures by Adding Synthesized Diisocyanate Compatibilizers

**Lerdlaksana Ubonnut, Supakanok Thongyai, Piyasan Praserthdam**

*Faculty of Engineering, Department of Chemical Engineering, Center of Excellence on Catalysis and Catalytic Reaction Engineering, Chulalongkorn University, Bangkok 10330, Thailand*

Received 5 May 2006; accepted 30 November 2006
DOI 10.1002/app.25945
Published online in Wiley InterScience (www.interscience.wiley.com).

ABSTRACT: Immiscible and incompatible binary blends of commercial polypropylene (PP)/polyethylene (PE) display poor mechanical properties. The addition of compatibilizer to reinforce and enhance an adhesion at the interfaces between PE–PP mixtures has been conducted. The compatibilizer chosen was in the group of Ziegler–Natta's PE–PP block copolymer with diisocyanate linkage. The effects of adding the compatibilizers were assessed by morphology studies, thermal analysis, and mechanical testing. DSC curves of crystallization and FTIR provided evidences to support the formation of PP/PE block copolymer. Significant improvements in the mechanical properties of 50/50 PE/PP blends containing compatibilizer have been noted. © 2007 Wiley Periodicals, Inc. J Appl Polym Sci 000: 000–000, 2007

Key words: PE/PP blend; polyethylene-polypropylene block copolymer; compatibilizer

## INTRODUCTION

Polyethylene (PE) and polypropylene(PP) are among the most common plastic wastes, because they are among the most frequently used commercial plastics in our daily lives as well as in industries.[1] It is impossible and not appropriate to identify and totally separate the waste mixtures of these two polymers. Usually, their waste mixture can recycle as mixed waste plastics in the form of blends. This reuse approach is attractive, because it avoids the difficult task of separation. As a consequence, academic and industrial interest in virgin and recycled polymer blends is rapidly expanding.

Unfortunately, the incompatibility between PE and PP has already been reported by various authors.[2] The strong phase separation leading to a coarse-phase structure and the low interfacial adhesion between the phases is responsible for a decrease in mechanical properties especially related to its morphology, including impact strength, strain at break, and ductile to brittle transition. According to Shanks,[3] the immiscibility between the phases makes the rule of mixtures ineffective in predicting some properties of interest.

To overcome this difficulty, the usages of various coupling agents have been reported. Incorporating a compatibilizer into a multiphase system generally leads to a fine phase structure and results in the enhanced interfacial adhesion. Among others,[4–6] Yang[7] showed that the addition of a commercial ethylene/propylene block copolymer improved the ductility of LDPE/PP blends, particularly for PP-rich blends. Bertin and Robin[8] studied and characterized virgin and recycled LDPE/PP blends and the usage of compatibilizing agents, such as ethylene–propylene–diene monomer (EPDM) copolymer or PE-*g* (2-methyl-1,3-butadiene) graft copolymer, to enhance their impact strength and elongation at break. Claudia and Agnes showed the partial compatibility of the PP/HDPE reflected in the improvement of tensile strength and elongation by the addition of extracted recycled PP.[9] Although this may solve the compatibility problem, the use of compatibilizers adds cost to the recycled product, usually resulting in less of interest from the recycling sector.

In this work, we try to synthesize the cost-effective compatibilizer in simple system that can improve the mechanical properties of PE/PP mixtures. Thus, we applied the rapid reaction between a polyfunctional isocyanate and a hydroxyl-terminated oligomer leads to urethane linkage. Consequently, the addition of Ziegler–Natta PE/PP-block copolymer synthesized by diisocyanate has the ability to reinforce the PE–PP mixtures as it is expected. Thermodynamically, the PP-*b*-PE will sit at the interface between the two components. In this work, the morphology, thermal

*Correspondence to:* S. Thongyai (supakanok.t@chula.ac.th).

Contract grant sponsor: Graduate school of Chulalongkorn University.

properties, and tensile properties of PP/PE blends were evaluated.

## EXPERIMENTAL

### Chemicals

Commercially graded PP and PE were donated from Thai Polyplastic Industry. Polymerization-grade propylene and ethylene were donated from National Petrochemical, Thailand. The $AlEt_3$ (TEA) and MDI were donated from Bangkok Polyethylene, Thailand. The $TiCl_4$ were purchased from Merck. Anhydrous $MgCl_2$ was supplied from Sigma-Aldrich, phthalic anhydride, diethylphthalate (DEP, used as an internal donor), and *n*-decane were purchased from Fluka Chemie A.G., Switzerland. Hexane was donated from Exxon Chemical, Thailand. It was purified by refluxing over sodium/benzophenone under argon atmosphere prior to use. Ultra high purity (UHP) argon (99.999%) and oxygen (UHP) was obtained from Thai Industrial Gas and was further purified by passing through molecular sieves 3Å, BASF catalyst R3-11G, NaOH, and phosphorus pentoxide ($P_2O_5$) to remove traces of oxygen and moisture.

All operations were carried out under an inert atmosphere of argon using a vacuum atmosphere glove box and/or standard Schlenk techniques.

### Catalyst preparation

A catalyst of type $TiCl_4$/DEP/$MgCl_2$ was synthesized in the following manner. About 0.476 g of anhydrous $MgCl_2$ was added to 2.5 mL of *n*-decane. This suspension was treated with 2.34 mL of 2-ethylhexanol and 0.1089 g of phathalic anhydride at 130°C. It was stirred until the $MgCl_2$ was dissolved. $TiCl_4$ (20 mL) was added dropwise at −20°C with subsequent treatment of the solution in the presence of 0.26 mL of DEP at 110°C for 2 h. The resulting solid product was separated by filtration and the addition of 20 mL of $TiCl_4$ was repeated at room temperature. After keeping the solution at 120°C for 2 h, this slurry was siphoned-off and washed twice with 10 mL of *n*-decane and thrice with 10 mL of hexane, respectively. The catalyst was dried under vacuum for 30 min at 40°C and contained 3% Ti.

### Polymerization reaction

#### PE and PP terminal hydroxyl group

The propylene polymerization and ethylene polymerization reactions were carried out in a 100-mL semi-batch stainless steel reactor equipped with magnetic stirrer. About 26.55-mL hexane, 0.01 g catalyst (Al/Ti molar ratio = 167), and 3.45-mL TEA were introduced into the reactor and stirred for 5 min at room temperature in the atmospheric glove boxes. Followed by that, the reactor was put in liquid nitrogen immediately to stop the reaction between the catalyst and cocatalyst. After the solution was frozen for 15 min, the reactor was evacuated for 3 min to remove argon. The reactions were conducted at 60°C and the polymerization was started by continuous feeding of ethylene (propylene) at constant pressure of 50 psi for 1 h. Then the polymerization was stopped by directly bringing into contact with oxygen gas at room temperature followed by precipitation in hydrochloric acid solution in methanol and dried at room temperature.

#### PE block PP copolymerization

Copolymerization was carried out in a glass reactor equipped with magnetic stirrer. PE and PP-containing hydroxyl group 50/50 wt % were added and dissolved in *o*-dichlorobenzene at 120°C. Followed by that excess MDI was dropped in the solution that remained stir for 1 h. The solution was washed with excess methanol and polymer was filtered and dried.

### Blend and molding preparation

The melt mixing method was performed in digital hot plate stirrer at 220°C, further kept for 5 min at 300°C, and annealed at 200°C for 20 min before the experiments[20] to allow the equilibrium and ensure the migration of the PE-*b*-PP to the interfaces. All blends were prepared with 50 wt % of commercial grade PE and 50 wt % of commercial grade PP (PE/PP), because PE/PP will become the easiest phase-separated and large amount of interfaces obtained. When the block copolymer was used, 3 wt % of the block copolymer was added base on the total weight of the 50/50 blend. And then, the block copolymer was added in PE/PP blend for 3, 6, 12, and 20 wt %. All polymer blends were molded with the LAB TECH hydraulic hot press LP-50M/C 9701.

### Measurements and characterization of block copolymers and blends

Infrared survey spectra were recorded with FTIR (IFS28). The scanning ranged from 400 to 4000 $cm^{-1}$ on the pallet sample of KBr powder (to hold the powder samples as a blank) with scanning 12 times.

The molecular weight and its distribution were determined by using GPC Model: Waters 2000 Column: Styragel HT6E with 1,2,4-trichlorobenzene as a solvent at 135°C.

The melting temperatures of the block copolymer-added polymer blends were determined with a PerkinElmer DSC-Pyris Diamond over the range −60 to

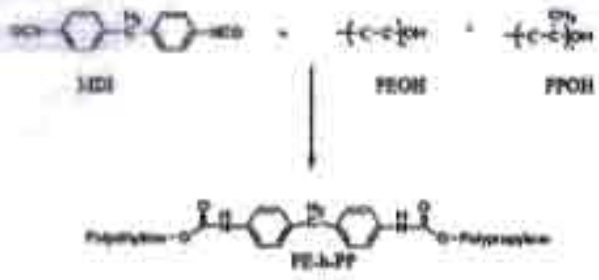


Scheme 1

200°C of scanning rate 40°C/min under nitrogen atmosphere.

Tensile properties were characterized using an Instron universal testing machine with a test speed of 12.5 mm/min. The tests were conducted according to ASTM D 882-02.

The morphologies of all block copolymers were investigated by JSM-5410LV Scanning Microscope. The samples for SEM analysis were coated with gold particles by ion-sputtering device to provide electrical contact to the specimens.

## RESULTS AND DISCUSSION

### Chain structure of PE/PP block copolymer diisocyanate linkage

On the basis of this result, a plausible products of the block copolymerization are proposed as shown in Scheme 1. S1

In addition, besides PE-*b*-PP, there have others two byproducts of the reaction, which are PE-*b*-PE and PP-*b*-PP. Moreover, there are other two products (urea end chain with hydrogen (not hydroxyl and OH) are PE, PP, and the small amount of remaining reactant, that is, PEOH and PPOH. The fractions of these byproducts are hardly to be quantified and it cannot be completely fractionated by solvent extraction. Thus, unidentified fraction distribution of the block copolymers will be along with what is identified as PE-*b*-PP throughout this study. However, the mixture identify as PE-*b*-PP had good phase binding with the melted blend of PP/PE that can be seen in SEM photo (Figs. 3 and 4). Consequently, the mixture of PE-*b*-PP copolymer in this study (PE-*b*-PP, and various sizes of PP and PE) comprised the phases that will dissolve in the melted blend of PP/PE without any difficulty. F3 F4 AQ3

### Characterization of PE-*b*-PP and their blends

From GPC results, the PE-*b*-PP has a wide molecular weight distribution resulted from the reaction of wide MWD of PPOH and PEOH with diisocyanate. To confirm the reaction that contribute to the block copolymer of PE-*b*-PP in this system, the IR spectrum of block copolymer obtained at 25°C is illustrated in Figure 1. The peak of isocyanate (NCO) transmittance is 1530 $cm^{-1}$, $\nu_{C=O}$ MDI = 1711 $cm^{-1}$, $\nu_{NH}$ = 3404, 1599, and 814 $cm^{-1}$. Thus, IR spectrum has identified the diisocyanate linkage in PE-*b*-PP copolymer structure. Moreover, the binding properties of PE-*b*-PP can be confirmed in SEM photo (Figs. 3 and 4) to ensure the abilities of our compatibilizer. F1

As shown in Table I, the effects of adding isocyanate compatibilizer can be clearly assured by their blends' properties. The PEOH has larger molecular weight compared to PPOH. Consequently, the molecular weights of PE-*b*-PP are higher than PPOH and change according to the isocyanate reaction. The *MI* T1

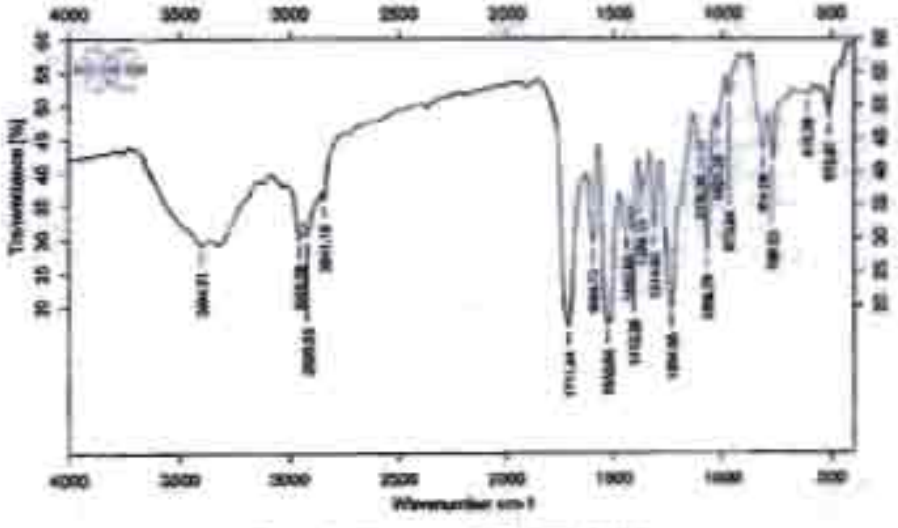


Figure 1 IR spectra of PE-*b*-PP at 25°C.

**TABLE I**
**Characterization of Polymer**

| Polymer | Mw[a] ($\times 10^{-4}$) | MWD[a] | Heating 1 (°C)[b] | | | | Cooling (°C)[b] | | | Heating 2 (°C)[b] | | | |
|---|---|---|---|---|---|---|---|---|---|---|---|---|---|
| | | | $T_{m1}$ | $T_{m2}$ | $T_g$ | $\Delta H_1$ | $T_{c1}$ | $T_{c2}$ | $\Delta H_2$ | $T_{m1}$ | $T_{m2}$ | $T_g$ | $\Delta H_3$ |
| PEOH | 117.3 | 7.5 | 145 | Nd | Nd | 181.4 | 110 | Nd | 123.6 | 137 | Nd | Nd | 118.9 |
| PPOH | 39.5 | 8.7 | Nd | 156 | −5 | 40.7 | 100 | Nd | 58.8 | Nd | 154 | −5 | 51.4 |
| PE-*b*-PE | Na | Na | 135 | Nd | Nd | 255.4 | 108 | Nd | 83.2 | 132 | Nd | Nd | 84.1 |
| PP-*b*-PP | Na | Na | 93 | 158 | −7 | 32.5 | 102 | Nd | 28.7 | Nd | 153 | −8 | 29.7 |
| PE-*b*-PP | 58.3 | 12.5 | 130 | 153 | −6 | 71.7 | 113 | 120 | 96.7 | 129 | 152 | −7 | 59.3 |
| PE/PP | 32.4 | 6.1 | 135 | 151 | −6 | 68.3 | 98 | 110 | 67.1 | 135 | 151 | −6 | 64.7 |
| 3%PEbPP | Na | Na | 136 | 163 | Nd | 131.6 | 111 | Nd | 133.7 | 134 | 164 | Nd | 137.3 |
| 6%PEbPP | Na | Na | 138 | 166 | Nd | 137.9 | 109 | Nd | 134.7 | 138 | 164 | Nd | 137.8 |
| 12%PEbPP | Na | Na | 138 | 165 | Nd | 122.9 | 109 | Nd | 122.3 | 136 | 163 | Nd | 122.3 |
| 20%PEbPP | Na | Na | 137 | 164 | Nd | 119.9 | 109 | Nd | 120.9 | 136 | 164 | Nd | 113.9 |

Na, not available.
Nd, not detected.
[a] Determined by gel permeation chromatography, PS standard.
[b] Determined by DSC, $\Delta H$ = (J/g).

of the melted blend of pure PE/PP is lower than all of the PE-*b*-PP addition samples, and this implied that the cystallinity of melted blend of pure PE/PP is increased when added with PE-*b*-PP. In other words, the copolymer enhanced the crystallization of both PE and PP in the melted blend of PE/PP. From the highest $\Delta H$, the largest percent of crystallinity is at 6% PE-*b*-PP in PE/PP. This may result in the best mechanical properties because of the formed crystal and contribute to the highest tensile strength. In addition, portion of $T_m$ that represented the PP crystal in PE/PP were increased from pure PE/PP in all the composition of added PE-*b*-PP. Usually, $T_m$ describing the quality of crystallinity in polymer blend form crystalline and decrease the entanglement in polymer blend). This can be concluded that the addition of our PE-*b*-PP alter both the quality and quantity of the crystallinity of PE/PP.

The chain structure of polymer blend and block copolymer was studied by DSC analysis of crystalline-segregated samples. After stepwise annealing of the samples at different temperatures, the long PP and PE segments can form crystalline lamellae of different thickness according to their sequential lengths, and these lamellae will melt at different temperatures.[11] By recording the endothermic curves of the polymer blend and block copolymer in a DSC scan, we are able to identify the sequential contribution of PE/PP blend and effects of the synthesized PE-*b*-PP in crystallinity of PE/PP.

The $T_g$ of the block copolymer should exhibit the glass transition of each of the respective homopolymer component as same as polymer blends.[12,13] According to Table I, the $T_g$ of PP[14] around −5°C indicate the cooperation of PP in the compatibilizer. Unfortunately, because of the low $T_g$ of PE at −110°C,[15] it cannot be detected in these DSC experiments. However, the crystalline melting characteristic of PE-*b*-PP shows the combination characteristics of both PE and PP. The melting peak at about 130–140°C corresponds to the melting temperature of PE crystal and the peak above 140°C corresponds to the melting temperature originate from PP crystal. The appearance of the curves of PE/PP blend and PE-*b*-PP is similar. In the cases of adding PE-*b*-PP to PE/PP blend, the melting temperatures of PP in PE/PP increase about 10°C (as shown in Table I). This may confirm the appearance of the synthesized PE-*b*-PP and the consequence of the addition of block copolymer.

## Morphology

According to SEM picture, it clearly shows the differences of the rough surface particles and the bridge formation with PP matrix of PE/PP blend, which continuously changed according to the concentration of PE-*b*-PP. The addition of PE-*b*-PP to PE/PP blend vividly shows the smaller phase particles size as increased concentrations. Many studies[16–19] on polymer alloys have shown that for multiphase polymer systems, the toughening effect is determined by two factors. First, the smaller the particles and the narrower the particles size distributions are, the better impact the strength is. Second, the stronger the adhesion between particle and the matrix, the better is the impact properties.

The SEM micrographs of compatibilized PE/PP blends (3, 6, 12, and 20% PE-*b*-PP) are shown in Figures 2 and 3. Figure 2 shows the tensile fracture of PE/PP and compatibilized PE/PP, while indicated that the interfacial adhesions, and therefore the compatibility of the PE and PP phases is better than the uncompatibilized PE/PP. In room temperature fracture experiments, the PE is in the form of tough rubbery polymer compared to PP. These might be shown as the stretch rubbery structure in the blends. The cryogenic fracture of the similar blends in Figure 3 will result in the clear domain size because at the

F2

J_ID: Z8E Customer A_ID: 25945 Date: 15-FEBRUARY-07 Stage: I Page: 5



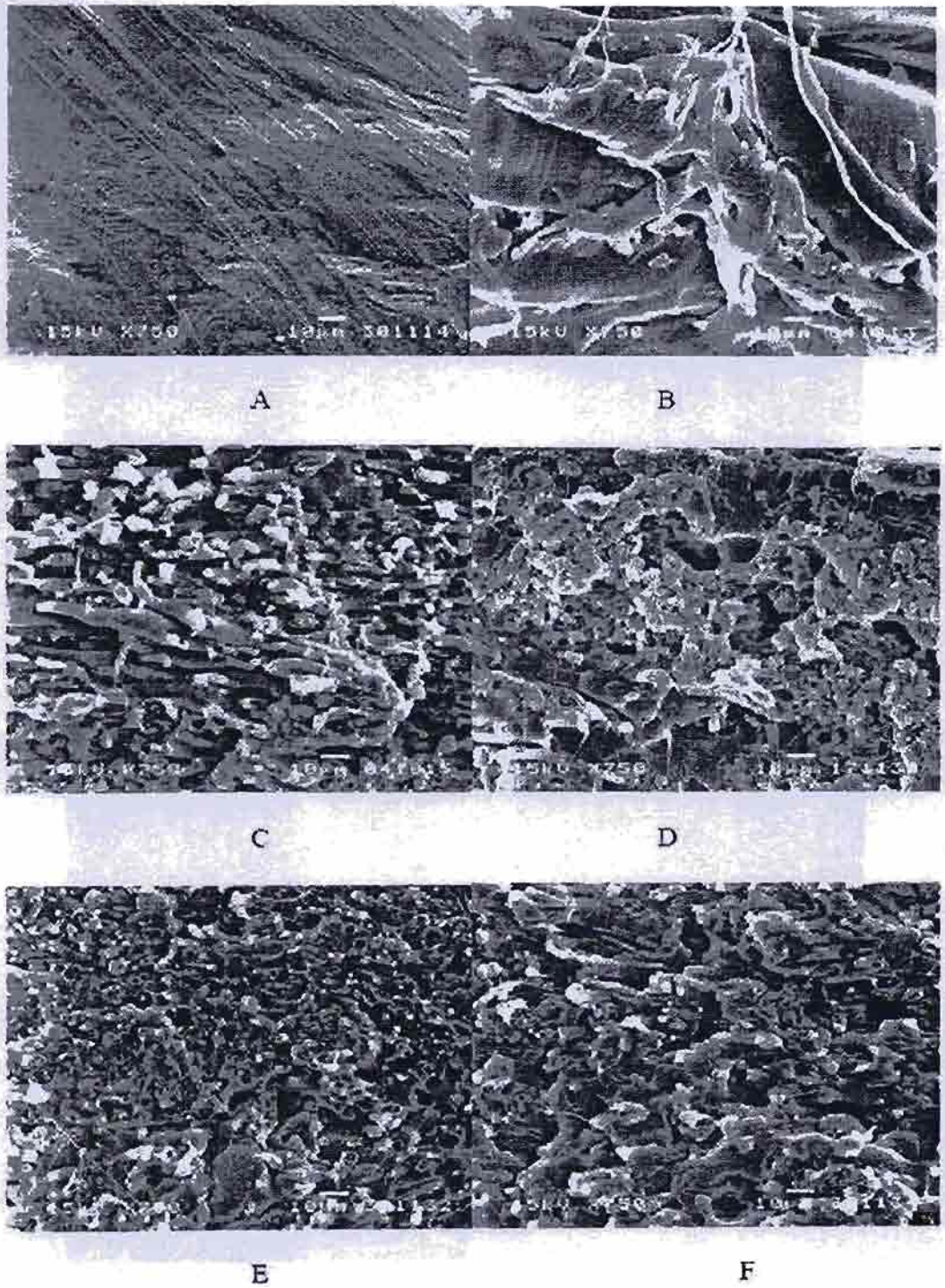

**Figure 2** SEM of tensile fracture surface of (a) PP, (b) PE/PP blend, (c) PE/PP+ PEbPP3%, (d) PE/PP+ PEbPP6%, (e) PE/PP+ PEbPP12%, and (f) PE/PP+ PEbPP20%.

cryogenic temperature both PE/PP are in the glassy states and the fractures cut directly to the cross sections of the segregation size in the blends.

In Figure 3, the cryogenic fracture of PE/PP and compatibilized PE/PP indicated clearly decrease in domain sizes (dispersion of PE in PP) and finer parti-



ID: 40456 Date: 15/2/07 Time: 00:33 Path: J:/Production/APP#/VOL00000/070132/3B2/C2APP#070132

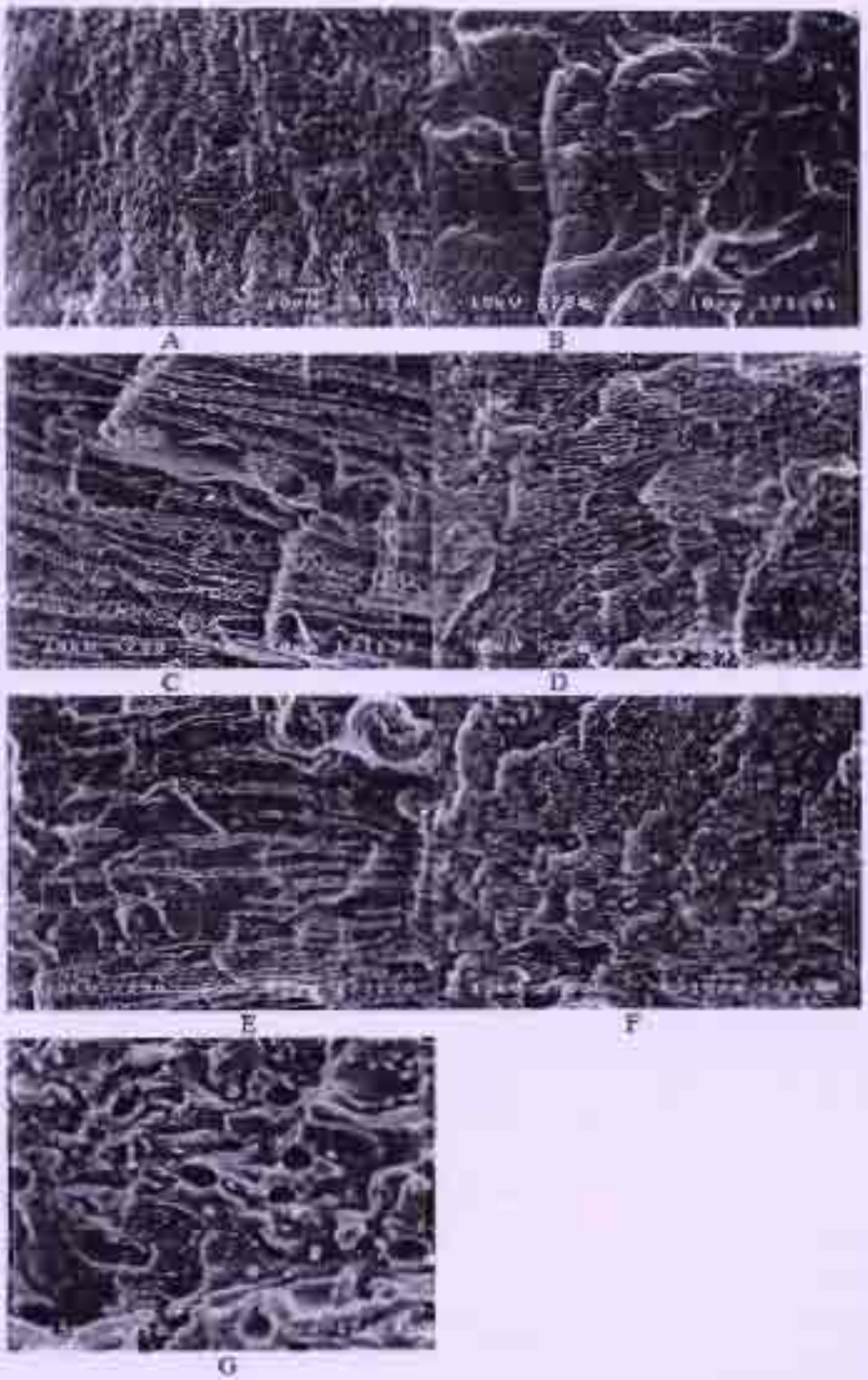


Figure 3 SEM of cryogenic fracture surface of (a) PE, (b) PP, (c) PE/PP blend, (d) PE/PP+ PEbPP3%, (e) PE/PP+ PEbPP6%, (f) PE/PP+ PEbPP12%, and (g) PE/PP+ PEbPP20%.

cle size distributions when adding more PE-b-PP in the blends. As might be confirmed by the SEM, the phase segregation decrease deliberately but the clear second dots of PE/PP are captured in the 12% and 20 wt % PE-b-PP, which might be the reason for the weaker interfacial ability than the 6 wt % PE-b-PP.

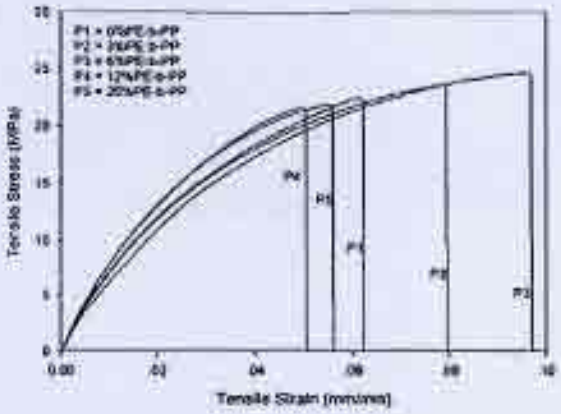


Figure 4 Additive effect of PE-*b*-PP to PE/PP blend on stress–strain behavior at 25°C.

Those samples have lower tensile properties than the 6 wt % PE-*b*-PP. These phenomena can confirm mechanical properties results.

### Mechanical properties

The results of tensile stress tests are shown in Figure 4 and Table II. As the concentration of PE-*b*-PP in melted blend of pure PE/PP increased, both the tensile strength and the elongation at break increased. These show that the addition of PE-*b*-PP to PE/PP can improve the reinforcement of polymer by increasing the interfacial adhesion between PE and PP. At 6% PE-*b*-PP in PE/PP, the highest tensile stress of the blend occurred, which resulted from more stiffness and toughness of the samples. Thus, the tensile properties of PE-*b*-PP in PE/PP were in agreement with DSC results as we discussed earlier that the 6 wt % PE-*b*-PP has the most reinforcement characteristics. The reasons of decreasing tensile strength and elongation at break at 12 and 20% PE-*b*-PP contents might be because of the lower percent crystal in the samples together with the increase of PE, PP pure from PE-*b*-PP that have the higher molecular weight than the commercial PE/PP. The amount of high molecular weight might result in the more incompatible of PE/PP. As usual, the portion of high molecular weight in the blend will result in phase separation of the high molecular weight species easier than the low molecular weight portions.[20] The SEM results supported what can be found in tensile testing. As the consequence, this can be concluded that the addition of our PE-*b*-PP will have the optimum at 6 wt % PE-*b*-PP.

TE2

TABLE II
Summary of Mechanical Properties

| Sample | Modulus (MPa) | Tensile strength (MPa) | Elongation (%) |
|---|---|---|---|
| PE/PP | 879.89 | 22.46 | 6.2 |
| 3%PE-*b*-PP | 782.19 | 23.63 | 8.0 |
| 6%PE-*b*-PP | 763.14 | 24.67 | 9.7 |
| 12%PE-*b*-PP | 927.01 | 21.59 | 8.1 |
| 20%PE-*b*-PP | 854.27 | 21.88 | 5.6 |

## CONCLUSIONS

A new synthesis method of PE-*b*-PP copolymer by converting the H-terminated chain ends to hydroxyl-terminated ones and blocking with diisocyanate is performed by the effective compatibilizer for immiscible blend of PE/PP. The diisocyanate linkages of PE-*b*-PP copolymers were confirmed by IR, which indicated that PE-*b*-PP copolymers occurred in the blocking reaction. The effects of PE-*b*-PP copolymers on the morphology of PE/PP blends were investigated by SEM with image analysis. The presence of the block copolymer dramatically reduced the phase size. Furthermore, the mechanical properties, such as tensile strength, elongation at break, and crystallinity, have been improved because of PE-*b*-PP copolymers. The phase-binding phenomena happened because the PE-*b*-PP contained PE and PP segments, which attached and bound the PE/PP segregate phase blend, leading to superior properties via changing morphology than the normal mixing blend without PE-*b*-PP. As confirmed by DSC, the compatibilized blends showed the increase of cystallinity percentage. The optimum content of compatibilizer is 6 wt % PE-*b*-PP, which shows the best optimal values from DSC, tensile tests, and SEM results.

The author thanks the Bangkok Polyethylene for the GPC characterizations and thank the Natural Petrochemical for supplying the ethylene and propylene gas. Furthermore, we like to thank MEKTEC manufacturing (Thailand) for supporting the characterize equipments and Ms. Nongnaphat for IR analysis.

### References

1. Patal, D. R.; Vinson, C. E.; Locke, C. E. Polym Eng Sci 1973, 13, 202.
2. Tho, J. W.; Rudin, A.; Kwong, J. C. Adv Polym Tech 1994, 13, 1.
3. Shanks, R. A.; Li, J.; Chen, F.; Amarasinghe, G. Chin J Polym Sci 2000, 18, 263.
4. Radonjic, G.; Cubeljak, N. Macromol Mater Eng 2002, 287, 122.
5. Androeopoulos, A. G.; et al. J Macromol Sci Pure 1999, 36, 1113. AQ4
6. Vaccaro, L.; Dibenedetto, A. T.; Huang, S. J. J Appl Polym Sci 1997, 63, 275.
7. Yang, M. B.; Wang, K.; Ye, L.; Mai, Y. W.; Wu, J. S. Plast Rubber Compos 2003, 32, 27.
8. Bertin, S.; Robin, J. J. Eur Polym J 2002, 38, 2255.
9. Claudia, M. C.; Agnes, F. J App Polym Sci 2001, 80, 1305.